

Contents lists available at ScienceDirect

Calphad

journal homepage: www.elsevier.com/locate/calphad





Analytically differentiable metrics for phase stability

Courtney Kunselman ^{a,*}, Brandon Bocklund ^b, Axel van de Walle ^c, Richard Otis ^d, Raymundo Arróyave ^{a,e,f}

- ^a Department of Materials Science and Engineering, Texas A&M University, College Station, TX 77843, USA
- ^b Materials Science Division, Lawrence Livermore National Laboratory, Livermore, CA 94550, USA
- ^c School of Engineering, Brown University, Providence, RI 02912, USA
- d Engineering and Science Directorate, Jet Propulsion Laboratory, California Institute of Technology, Pasadena, CA 91109, USA
- ^e Department of Mechanical Engineering, Texas A&M University, College Station, TX 77843, USA
- f Department of Industrial and Systems Engineering, Texas A&M University, College Station, TX 77843, USA

ARTICLE INFO

Keywords: CALPHAD Equilibrium calculations Thermodynamics

ABSTRACT

In this work, a long-established but sparsely documented method of obtaining semi-analytic derivatives of thermodynamic properties with respect to equilibrium conditions is briefly reviewed and rigorously derived. This procedure is then leveraged to construct general forms of derivatives of the residual driving force, a metric for measuring phase stability used in CALPHAD model optimization, with respect to overall system and individual phase compositions. Applied examples – calculating heat capacity in the Al-Fe system, thermodynamic factors in the Nb-V-W system, and residual driving force derivatives in the Ni-Ti system – demonstrate the versatility, accuracy, and extensibility of this method. Using the developed method, residual driving force gradients can be applied directly in CALPHAD model optimizers, as well as in materials design frameworks, to identify regions of phase stability with an efficient, gradient-based approach.

1. Introduction

Thermodynamics provides an elegant and rigorous analytical framework for describing how the internal state of a given system changes as a function of changes in external conditions. Application of these foundational principles to explain and predict the behavior of real systems led to the development of the Calculation of Phase Diagram (CALPHAD) method [1]. In this method, parametric models for the Gibbs energies of individual phases are built as functions of temperature, pressure, and constitution and fit to empirical and/or computational data. Further independent variables and corresponding physics can be added to the models if the system experiences additional types of work.

Given a set of external conditions, the equilibrium state of the system is then determined through a constrained minimization of the total Gibbs energy. Constraints can be external—applying to the system as a whole—or internal—applying to an individual phase—and they range from setting the equilibrium temperature and composition of the system, to assigning the phase fraction of a given phase or enforcing a variety of internal and external conservation laws. The outcome of this minimization is the overall specification of the system and internal phase degrees of freedom, such as phase fraction and sublattice site fractions, respectively, at the thermodynamic equilibrium state corresponding to the provided external conditions.

While this outcome is extremely useful for applications requiring the equilibrium Gibbs energy description and/or corresponding external and internal degrees of freedom of the equilibrium system, it is not easily extensible to all other equilibrium thermodynamic properties that may be of interest. In theory, properties derived from the fundamental thermodynamic equation or its Legendre transforms can be obtained by taking derivatives of the Gibbs energy with respect to the appropriate external conditions. However, solving the constrained optimization problem introduces dependent variables into the equilibrium model of the Gibbs energy, making the recovery of analytic expressions for the dependence of these degrees of freedom on external conditions generally nontrivial. Thus, analytic expressions for equilibrium thermodynamic properties outside of Gibbs energy are not always readily evident at the conclusion of an equilibrium calculation.

Of course, derivatives of the Gibbs energy can be approximated numerically. However, these approximations can be both computationally expensive for high-throughput, multi-component calculations, and extremely sensitive to even small discontinuities in the underlying thermodynamic functions. Seeking to avoid numeric differentiation and recognizing that all necessary information to calculate analytic derivatives is encoded in the minimized Gibbs energy functional, Bo

E-mail address: cjkunselman18@tamu.edu (C. Kunselman).

^{*} Corresponding author.

Jansson developed and implemented the "dot derivative" method in the commercial Thermo-Calc software in the 1980s [2,3]. More recently, open-source thermodynamic equilibrium calculation software such as OpenCalphad [4] and PyCalphad [5] also allow users to leverage the dot derivative method. As explained in [6,7], the dot derivative approach allows for point queries of the analytic derivative of thermodynamic quantities with respect to external conditions at the conclusion of an equilibrium calculation through the application of an adjoint-like procedure [8] in which the assigned external conditions are treated as design variables. Since the term dot derivative is also used to refer to derivatives with respect to time in many engineering applications, the remainder of this work will refer to this technique of calculating analytic thermodynamic derivatives at equilibrium as the "Jansson derivative" method.

The specific procedure for calculating a Jansson derivative can vary based on the applied Gibbs energy minimization method. In [6], Larsson and Jansson provide a rigorous mathematical description of a general Jansson derivative method that couples well with a Newton-Raphson minimizer which optimizes phases' internal degrees of freedom and overall system constraints all in one step for each iteration [9]. In [7], Sundman et al. document a Jansson derivative procedure that couples well with a sequential quadratic programming (SQP) minimizer defined by the Lagrange–Newton method in which the optimization of internal phase degrees of freedom are decoupled for each phase through fixing the values of the overall system constraints at the newly-calculated value for that iteration [10,11]. However, Sundman et al. [7] only outline the procedure for taking a derivative with respect to a potential, and they do not provide rigorous proof for why the method works.

The ability to efficiently calculate analytic derivatives of thermodynamic properties at equilibrium with respect to conditions of the equilibrium calculation is extremely useful for a variety of applications. Basic applications of these derivatives include calculating properties such as heat capacity, thermal expansion, and isothermal compressibility as they are defined in terms of derivatives of the thermodynamic potentials. More sophisticated applications include the calculation of derivatives of temperature with respect to composition—or vice versa-in order to explore the behavior of phase boundaries in highdimensional systems. Additionally, thermodynamic factors, or derivatives of chemical potential with respect to composition, can be cleverly employed to compute curvature of the Gibbs energy surface in composition space. Recent publications treat CALPHAD model parameters as thermodynamic potentials to demonstrate how Jansson derivatives with respect to these parameters can be used for sensitivity analysis [12] and uncertainty quantification (UQ) [13]. Looking forward, UQ methods similar to that employed in [13], which showed drastic improvements in efficiency over widely-used Monte Carlo approaches, could be applied to systems described by more complex models such as the modified quasichemical model [14]. Similarly, analytic gradients of error functions with respect to model parameters would allow for efficient gradient-based optimization approaches, compared to stateof-the-art approaches using least-squares [2], or "black box" Bayesian inference through Markov Chain Monte Carlo [15]. Furthermore, the residual driving force can also be viewed as a differentiable metric for phase stability for the problem of alloy design in high-dimensional composition spaces, and derivatives of this quantity with respect to composition would allow for much more efficient searches through vast alloy design spaces [16,17].

2. Theory and definitions

2.1. Modeling the Gibbs energy

The foundational elements of thermodynamic calculations within the CALPHAD method are the parametric models that describe the Gibbs energies of individual phases. The construction of these models is not constrained to a singular approach. However, given that equilibrium in a closed system at constant temperature and pressure is characterized by a minimum in the Gibbs energy, these models are typically formulated as functions dependent on temperature (T), pressure (P), and constitution (Y)

$$G_M^{\alpha}(T, P, \mathbf{Y})$$
 (1)

where G_M^{α} is the Gibbs energy per mole formula unit of phase α . Note that in Eq. (1) and throughout the rest of this work, italic typeface indicates a scalar value while boldface indicates a vector quantity. The overall Gibbs energy is then given by

$$G = \sum_{\alpha} \mathcal{N}^{\alpha} G_{M}^{\alpha} \tag{2}$$

where \mathcal{N}^{α} is the moles of formula units of phase α . Defining G_{M}^{α} in terms of constitution instead of composition allows for the modeler to account for internal degrees of freedom within a phase. If the Compound Energy Formalism (CEF) [18] is used, these internal degrees of freedom are modeled using sublattices. Then, for phase α , y_{is}^{α} is the site fraction of constituent i on sublattice s. Similar to composition, the sum of site fractions for a given sublattice must equal one, creating one dependent site fraction on each sublattice. Site fractions are related to M_{A}^{α} , moles of component A per mole formula unit of phase α , through

$$M_A^{\alpha} = \sum_s a_s^{\alpha} \sum_i b_{Ai} y_{is}^{\alpha} \tag{3}$$

where a_s^{α} is the ratio of sites on sublattice s and b_{Ai} is the moles of component A in a mole of constituent i. M_A^{α} is then connected to the total moles of component A, N_A through

$$N_A = \sum_{\alpha} \mathcal{N}^{\alpha} M_A^{\alpha},\tag{4}$$

and to G_M^{α} through

$$G_M^{\alpha} = \sum_{i} M_A^{\alpha} \mu_A \tag{5}$$

where μ_A is the chemical potential of component A. The overall mole fraction of component A, x_A , is then given by

$$x_A = \frac{N_A}{\sum_B N_B} = \frac{\sum_\alpha \mathcal{N}^\alpha M_A^\alpha}{\sum_\alpha \mathcal{N}^\alpha \sum_B M_B^\alpha}.$$
 (6)

2.2. Differentials and derivatives

In thermodynamics, many important properties of a system are related through partial derivatives. A common way of representing these relationships is through a total differential form of one quantity in terms of independent variables of interest. For example, the total differential of enthalpy (H) as a function of temperature, pressure, and moles of components for an otherwise simple system is given by

$$dH = \left(\frac{\partial H}{\partial T}\right)_{P,\mathbf{N}} dT + \left(\frac{\partial H}{\partial P}\right)_{T,\mathbf{N}} dP + \left(\frac{\partial H}{\partial \mathbf{N}}\right)_{T,P} d\mathbf{N}. \tag{7}$$

In this total differential form, all influences of how H varies with a given independent variable are captured in its corresponding partial derivative. That is, there are no lurking dependent variables.

Now, it is commonly understood that the partial derivative of enthalpy with respect to temperature in Eq. (7) is equal to the isobaric heat capacity, C_P :

$$\left(\frac{\partial H}{\partial T}\right)_{P,\mathbf{N}} = C_P. \tag{8}$$

However, if the model described in Section 2.1 is used to define enthalpy of the system as

$$H = \sum \mathcal{N}^{\alpha} H_M^{\alpha} \tag{9}$$

where $H_M^\alpha = G_M^\alpha + TS_M^\alpha$, H is now a function of independent variables T, P, Y, and \mathcal{N} . If there is specific interest in the functional form of H

at equilibrium for fixed T, P, and N, the procedure given in Section 3 outlines how numerical optimization techniques can be used to solve a point calculation for Y and \mathcal{N} . That is, at equilibrium, \mathcal{N} and Y become dependent variables which are functions of independent variables T, P, and N. Additionally, because these dependent variables are being solved-for numerically, there are no readily evident analytic functional forms that can be substituted into the model of H in order to represent equilibrium H as a function of only independent variables. Thus, if the partial derivative of the model of H at equilibrium with respect to T is computed while holding P and N constant, the incorrect value of C_P would be calculated because contributions from changes in the amounts of phases or in the internal degrees of freedom of these phases that are caused by a change in temperature would not be taken into account.

The above discussion illustrates the need for a procedure that calculates the total derivative for models optimized to be at equilibrium. For the model of H at equilibrium, this would be

$$\frac{dH}{dT} = \frac{\partial H}{\partial T} + \frac{\partial H}{\partial \mathcal{N}} \frac{d\mathcal{N}}{dT} + \frac{\partial H}{\partial \mathbf{Y}} \frac{d\mathbf{Y}}{dT}.$$
 (10)

While analytic functional forms of all of the partial derivatives in Eq. (10) are straightforward to derive by taking the appropriate partial derivative of the unoptimized enthalpy displayed in Eq. (9), the total derivatives of the dependent variables need to be solved through another method because the minimizer only provides point calculations of the functional relationship between \mathcal{N} , Y, and T. Thus, the purpose of the Jansson derivative procedure is to solve for the total derivatives of the dependent variables with respect to a given condition of the equilibrium calculation.

Since lurking dependent variables are present in many quantities that are of interest to differentiate, this work will break from convention and represent derivatives of thermodynamic properties with respect to one independent variable while holding all other independent variables constant as total derivatives. Partial derivatives in this work will imply that all other variables (including any dependent variables apart from the quantity being differentiated) are held constant.

Interestingly, it can be shown for first derivatives of the Gibbs energy in a closed system that the contributions to the total derivative from the dependent variables sum to zero, leading to the partial derivative equaling the total derivative. This means that partial derivatives of G at equilibrium with respect to temperature and pressure provide enough information to produce analytic functional forms of entropy, enthalpy, and volume. A proof is presented in Appendix A.

3. Equilibrium calculations

This section provides a sprint through the Lagrange-Newton optimizer implemented in [4] and [5] for the constrained minimization of Gibbs energy. For a more detailed description, see [7].

3.1. The Lagrangian

As stated above, equilibrium calculations aim to minimize Eq. (2) subject to both internal phase and overall system constraints. Internal phase constraints include the set of site fractions corresponding to a given sublattice *s* summing to one:

$$1 - \sum_{i} y_{is}^{\alpha} = 0. {(11)}$$

Overall system constraints include mass balance when the system is closed:

$$N_A - \sum_{\alpha} \mathcal{N}^{\alpha} M_A^{\alpha} = 0. \tag{12}$$

Additional constraints (such as charge balance for phases with ions) are added as required for the specific system being minimized. Then,

through the method of Lagrange multipliers, the constraints are conveniently added as multiples of zero to the unconstrained objective function, resulting in the constrained Lagrangian:

$$L(\mathcal{N}, \mathbf{Y}, \boldsymbol{\mu}, \boldsymbol{\eta}) = \sum_{\alpha} \mathcal{N}^{\alpha} G_{M}^{\alpha} + \sum_{A} \mu_{A} \left(N_{A} - \sum_{\alpha} \mathcal{N}^{\alpha} M_{A}^{\alpha} \right) + \sum_{\alpha} \sum_{s} \eta_{s}^{\alpha} \left(1 - \sum_{i} y_{is}^{\alpha} \right)$$

$$(13)$$

where η and μ are the vectors of multipliers corresponding to the site fraction and mass balance constraints, respectively.

Calculating the gradient of L with respect to phase amount, site fraction, and the multipliers and setting that gradient equal to zero gives

$$\frac{\partial L}{\partial \mathcal{N}^{\alpha}} = G_M^{\alpha} - \sum_A M_A^{\alpha} \mu_A = 0, \tag{14}$$

$$\frac{\partial L}{\partial y_{is}^{\alpha}} = \mathcal{N}^{\alpha} \frac{\partial G_{M}^{\alpha}}{\partial y_{is}^{\alpha}} - \mathcal{N}^{\alpha} \sum_{A} \mu_{A} \frac{\partial M_{A}^{\alpha}}{\partial y_{is}^{\alpha}} - \eta_{s}^{\alpha} = 0, \tag{15}$$

$$\frac{\partial L}{\partial \eta_x^{\alpha}} = 1 - \sum_i y_{is}^{\alpha} = 0,\tag{16}$$

$$\frac{\partial L}{\partial \mu_A} = N_A - \sum_{\alpha} \mathcal{N}^{\alpha} M_A^{\alpha} = 0. \tag{17}$$

As Sundman et al. point out in [7], Eq. (14) implies that the mass balance constraint multiplier μ_A is the chemical potential of component A.

3.2. Building the phase and equilibrium matrices

To build the phase matrix, $\frac{\partial G_M^\alpha}{\partial y_i^\alpha}$ is expanded in a first-order Taylor series with respect to $T,\ P,$ and Y:

$$\frac{\partial G_{M}^{\alpha}}{\partial y_{is}^{\alpha}} = \frac{\partial G_{M}^{\alpha}}{\partial y_{is}^{\alpha}} + \frac{\partial^{2} G_{M}^{\alpha}}{\partial y_{is}^{\alpha} \partial T} \Delta T + \frac{\partial^{2} G_{M}^{\alpha}}{\partial y_{is}^{\alpha} \partial P} \Delta P + \sum_{t} \sum_{j} \frac{\partial^{2} G_{M}^{\alpha}}{\partial y_{is}^{\alpha} \partial y_{jt}^{\alpha}} \Delta y_{jt}^{\alpha}$$
(18)

where the derivatives on the right-hand side are evaluated at the current values of T, P, and Y, and the term on the left-hand side is the linear response of $\frac{\partial G_M^M}{\partial y_i^a}$ after some change in the independent variables. Substituting Eq. (18) into Eq. (15) and omitting phase and sublattice indices gives the system of equations for each phase:

$$\begin{pmatrix}
\frac{\partial^{2}G_{M}}{\partial y_{1}^{2}} & \frac{\partial^{2}G_{M}}{\partial y_{1}\partial y_{2}} & \dots & 1 & \dots \\
\frac{\partial^{2}G_{M}}{\partial y_{1}\partial y_{2}} & \frac{\partial^{2}G_{M}}{\partial y_{2}^{2}} & \dots & 1 & \dots \\
\vdots & & & & & & \\
1 & 1 & \dots & 0 & \dots \\
\vdots & & & & & \\
\sum_{A} \mu_{A} \frac{\partial M_{A}}{\partial y_{1}} - \frac{\partial G_{M}}{\partial y_{1}} - \frac{\partial^{2}G_{M}}{\partial y_{1}\partial T} \Delta T - \frac{\partial^{2}G_{M}}{\partial y_{1}\partial T} \Delta P \\
\sum_{A} \mu_{A} \frac{\partial M_{A}}{\partial y_{2}} - \frac{\partial G_{M}}{\partial y_{2}} - \frac{\partial^{2}G_{M}}{\partial y_{2}\partial T} \Delta T - \frac{\partial^{2}G_{M}}{\partial y_{2}\partial P} \Delta P \\
\vdots & & & & \\
0 & & & & \\
\vdots & & & & \\
0 & & & & & \\
\end{cases} .$$
(19)

Sundman et al. [7] name the matrix on the left-hand side the *phase matrix*. Denoting the entries in the inverted phase matrix as e_{ij}^a :

$$\begin{pmatrix} e_{11} & e_{12} & \dots \\ e_{21} & e_{22} & \dots \\ \vdots & & & \vdots \end{pmatrix} = \begin{pmatrix} \frac{\partial^2 G_M}{\partial y_1^2} & \frac{\partial^2 G_M}{\partial y_1 \partial y_2} & \dots & 1 & \dots \\ \frac{\partial^2 G_M}{\partial y_1 \partial y_2} & \frac{\partial^2 G_M}{\partial y_2^2} & \dots & 1 & \dots \\ \vdots & & & & & \vdots \\ 1 & 1 & \dots & 0 & \dots \\ \vdots & & & & & \end{pmatrix}, \tag{20}$$

the corrections for site fractions are expressed as

$$\Delta y_{is}^{\alpha} = c_{iG}^{\alpha} + c_{iT}^{\alpha} \Delta T + c_{iP}^{\alpha} \Delta P + \sum_{A} c_{iA}^{\alpha} \mu_{A}$$
 (21)

where c_{iG}^{α} , c_{iP}^{α} , c_{iP}^{α} , and c_{iA}^{α} are given by

$$c_{iG}^{\alpha} = -\sum_{j} e_{ij}^{\alpha} \frac{\partial G_{M}^{\alpha}}{\partial y_{j}^{\alpha}},\tag{22}$$

$$c_{iT}^{\alpha} = -\sum_{j} e_{ij}^{\alpha} \frac{\partial^{2} G_{M}^{\alpha}}{\partial y_{i}^{\alpha} \partial T},$$
(23)

$$c_{iP}^{\alpha} = -\sum_{i} e_{ij}^{\alpha} \frac{\partial^{2} G_{M}^{\alpha}}{\partial y_{i}^{\alpha} \partial P}, \tag{24}$$

$$c_{iA}^{\alpha} = \sum_{i} e_{ij}^{\alpha} \frac{\partial M_{A}^{\alpha}}{\partial y_{i}^{\alpha}}.$$
 (25)

As evidenced by Eq. (21), corrections to site fraction values for each phase are connected to movement of the overall system through changes in the system potentials. What Sundman et al. label as the equilibrium matrix system of equations calculates these new values as well as corrections to the phase amounts.

To start building the equilibrium matrix, G_M^{α} in Eq. (14) is expanded in a first-order Taylor series with respect to T and P:

$$G_M^{\alpha} = \sum_{A} M_A^{\alpha} \mu_A - \frac{\partial G_M^{\alpha}}{\partial T} \Delta T - \frac{\partial G_M^{\alpha}}{\partial P} \Delta P.$$
 (26)

Next, the differential of N_A in the mass balance constraints (Eqs. (12) and/or (17)) is computed and set equal to zero. Continuing with finite difference notation, this gives

$$\Delta N_A = \sum_{\alpha} \mathcal{N}^{\alpha} \Delta M_A^{\alpha} + \sum_{\alpha} \Delta \mathcal{N}^{\alpha} M_A^{\alpha} = 0. \tag{27}$$

Remembering that M^α_A is a function of Y and omitting sublattice indices, ΔM^α_A can be expressed as

$$\Delta M_A^{\alpha} = \sum_i \frac{\partial M_A^{\alpha}}{\partial y_i^{\alpha}} \Delta y_i^{\alpha}. \tag{28}$$

Inserting Eq. (21) into Eq. (28) gives

$$\Delta M_A^{\alpha} = \sum_i \frac{\partial M_A^{\alpha}}{\partial y_i^{\alpha}} \left(c_{iG}^{\alpha} + c_{iT}^{\alpha} \Delta T + c_{iP}^{\alpha} \Delta P + \sum_B c_{iB}^{\alpha} \mu_B \right), \tag{29}$$

and this relation is inserted into Eq. (27) to make it a function of the potentials.

If composition is specified as a condition, the differential of Eq. (6) is computed and set equal to zero. Once again continuing with finite difference notation, this gives

$$\Delta x_A = \frac{1}{\sum_{\alpha} \mathcal{N}^{\alpha} \sum_{B} M_B^{\alpha}} \left[\sum_{\alpha} \mathcal{N}^{\alpha} (\Delta M_A^{\alpha} - x_A \sum_{B} \Delta M_B^{\alpha}) + \sum_{\alpha} (M_A^{\alpha} - x_A \sum_{B} M_B^{\alpha}) \Delta \mathcal{N}^{\alpha} \right] = 0$$
(30)

where similar to Eq. (27), Eq. (29) is substituted for ΔM_A^{α} .

The equilibrium matrix system of equations is then constructed from Eqs. (26), (27), and (30) based on the specified conditions for the system. For example, a ternary A-B-C system with one stable phase in which temperature, pressure, amount of each component, and composition are conditions gives the linear system in Box I. Note that component x_C is the dependent composition variable and the second row of the equilibrium matrix (left-hand side) corresponds to a sum of Eq. (27) over all components. See [7] for many more examples.

Once the phase matrix and equilibrium matrix linear systems are established, suitable starting values for the set of stable phases and their corresponding site fractions are determined through either a stochastic or grid-based sampling strategy (Newton's method is sensitive to starting values, and appropriate sampling procedures are paramount to ensuring a global minimum is reached). The algorithm then iterates between the equilibrium matrix and phase matrix linear systems until corrections are sufficiently small, signaling that equilibrium has been reached.

4. Derivatives with respect to equilibrium conditions

As mentioned in Section 2.2, the purpose behind the Jansson derivative procedure is to solve for the total derivatives of the dependent variables of an equilibrium calculation with respect to a given equilibrium condition. In this section, the method will be derived for an arbitrary condition and then applied in examples for both a derivative with respect to a potential and a derivative with respect to a composition variable. The section concludes with applied examples for using these derivatives to calculate constant pressure heat capacity in the Al-Fe system and thermodynamic factors for the BCC phase in the Nb-V-W system.

4.1. Jansson derivatives with respect to an arbitrary equilibrium condition

Let K be the vector of external conditions, Y be the vector of site fractions for all stable phases, and W be the vector of overall systemdependent variables (e.g. the vector of unknowns in Eq. (31)). As their label implies, overall system-dependent variables are functions of external conditions, W(K). Similarly, Eq. (21) shows that site fractions are functions of conditions and overall system-dependent variables, Y(K, W). Thus, the total derivative $\frac{dy_{is}^{\alpha}}{dk_i}$ for some $y_{is}^{\alpha} \in Y$ and $k_j \in K$

$$\frac{dy_{is}^{\alpha}}{dk_{j}} = \frac{\partial y_{is}^{\alpha}}{\partial k_{j}} + \sum_{l} \frac{\partial y_{is}^{\alpha}}{\partial w_{l}} \frac{dw_{l}}{dk_{j}}$$
(32)

where the sum is capturing all contributions from dependent variables $w_l \in \mathbf{W}$. At the conclusion of an equilibrium calculation consisting of n iterations before converging, Y can be expressed as

$$\mathbf{Y} = \mathbf{Y}_{n-1} + \Delta \mathbf{Y}_n \tag{33}$$

where ΔY_n is the *n*th addition of the site fraction correction given in Eq. (21). Treating Y_{n-1} as a constant (i.e. as an arbitrary starting value for the nth iteration) allows Eq. (32) to be rewritten as

$$\frac{dy_{is}^{\alpha}}{dk_{j}} = \frac{d\Delta y_{is}^{\alpha}}{dk_{j}} = \frac{\partial \Delta y_{is}^{\alpha}}{\partial k_{j}} + \sum_{l} \frac{\partial \Delta y_{is}^{\alpha}}{\partial w_{l}} \frac{dw_{l}}{dk_{j}}$$
(34)

where Δy_{is}^{α} is given by Eq. (21) at equilibrium. While calculation of $\frac{\partial \Delta y_{is}^{\alpha}}{\partial k_{j}}$ is straightforward, calculating the total derivatives of **W** with respect to k_{j} requires a different approach. The strategy employed here entails setting up a system of equations similar to the equilibrium matrix linear system where the vector of unknowns is $\frac{d\mathbf{W}}{dk}$. To start, consider the differential form of Eq. (14).

$$dG_M^{\alpha} = \sum_A \mu_A dM_A^{\alpha} + \sum_A M_A^{\alpha} d\mu_A. \tag{35}$$

A more familiar way of expressing the differential of G_M^{α} is given by

$$dG_M^{\alpha} = \frac{\partial G_M^{\alpha}}{\partial T} dT + \frac{\partial G_M^{\alpha}}{\partial P} dP + \sum_A \mu_A dM_A^{\alpha}$$
 (36)

where M^{α}_{A} becomes the natural conjugate variable for μ_{A} due to the definition of G_M^{α} . Comparing Eqs. (35) and (36) reveals the following form of the Gibbs-Duhem equation:

$$\sum_{A} M_{A}^{\alpha} d\mu_{A} = \frac{\partial G_{M}^{\alpha}}{\partial T} dT + \frac{\partial G_{M}^{\alpha}}{\partial P} dP. \tag{37}$$

Dividing both sides of Eq. (37) by the differential of k_i (or, rather, recognizing the relationship between total derivative and differential

$$\sum_{A} M_{A}^{\alpha} \frac{d\mu_{A}}{dk_{j}} = \frac{\partial G_{M}^{\alpha}}{\partial T} \frac{dT}{dk_{j}} + \frac{\partial G_{M}^{\alpha}}{\partial P} \frac{dP}{dk_{j}}.$$
(38)

Next, taking the derivative of N_A from Eq. (17) with respect to condition k_i and setting it equal to zero gives

$$\frac{dN_A}{dk_j} = \sum_{\alpha} \frac{d\mathcal{N}^{\alpha}}{dk_j} M_A^{\alpha} + \sum_{\alpha} \mathcal{N}^{\alpha} \frac{dM_A^{\alpha}}{dk_j} = 0.$$
 (39)

$$\begin{pmatrix}
M_{A} & M_{B} & M_{C} & 0 \\
N \sum_{i} c_{iA} \sum_{D} \frac{\partial M_{D}}{\partial y_{i}} & N \sum_{i} c_{iB} \sum_{D} \frac{\partial M_{D}}{\partial y_{i}} & N \sum_{i} c_{iC} \sum_{D} \frac{\partial M_{D}}{\partial y_{i}} & \sum_{D} M_{D} \\
\frac{\sum_{i} c_{iA} \left(\frac{\partial M_{A}}{\partial y_{i}} - x_{A} \sum_{D} \frac{\partial M_{D}}{\partial y_{i}}\right) & \sum_{i} c_{iB} \left(\frac{\partial M_{A}}{\partial y_{i}} - x_{A} \sum_{D} \frac{\partial M_{D}}{\partial y_{i}}\right) & \sum_{i} c_{iC} \left(\frac{\partial M_{A}}{\partial y_{i}} - x_{A} \sum_{D} \frac{\partial M_{D}}{\partial y_{i}}\right) & \frac{M_{A} - x_{A} \sum_{D} M_{D}}{N \sum_{D} M_{D}} \\
\frac{\sum_{i} c_{iA} \left(\frac{\partial M_{B}}{\partial y_{i}} - x_{B} \sum_{D} \frac{\partial M_{D}}{\partial y_{i}}\right) & \sum_{i} c_{iB} \left(\frac{\partial M_{B}}{\partial y_{i}} - x_{B} \sum_{D} \frac{\partial M_{D}}{\partial y_{i}}\right) & \sum_{i} c_{iC} \left(\frac{\partial M_{B}}{\partial y_{i}} - x_{B} \sum_{D} \frac{\partial M_{D}}{\partial y_{i}}\right) & \frac{M_{A} - x_{A} \sum_{D} M_{D}}{N \sum_{D} M_{D}} \end{pmatrix}$$

$$\frac{\sum_{i} c_{iC} \left(\frac{\partial M_{B}}{\partial y_{i}} - x_{B} \sum_{D} \frac{\partial M_{D}}{\partial y_{i}}\right) & \sum_{i} c_{iC} \left(\frac{\partial M_{B}}{\partial y_{i}} - x_{B} \sum_{D} \frac{\partial M_{D}}{\partial y_{i}}\right) & \frac{M_{B} - x_{B} \sum_{D} M_{D}}{N \sum_{D} M_{D}} \end{pmatrix}$$

$$\frac{M_{B} - x_{B} \sum_{D} M_{D}}{N \sum_{D} M_{D}} = \begin{pmatrix} G_{M} \\ N \sum_{i} c_{iG} \sum_{D} \frac{\partial M_{D}}{\partial y_{i}} \\ \sum_{D} M_{D} & \sum_{D} M_{D} \end{pmatrix}$$

$$\frac{\sum_{i} c_{iC} \left(\frac{\partial M_{B}}{\partial y_{i}} - x_{A} \sum_{D} \frac{\partial M_{D}}{\partial y_{i}}\right)}{\sum_{D} M_{D}} = \begin{pmatrix} G_{M} \\ N \sum_{i} c_{iG} \left(\frac{\partial M_{B}}{\partial y_{i}} - x_{A} \sum_{D} \frac{\partial M_{D}}{\partial y_{i}}\right) \\ \sum_{D} M_{D} \end{pmatrix}$$

$$\frac{\sum_{i} c_{iC} \left(\frac{\partial M_{B}}{\partial y_{i}} - x_{B} \sum_{D} \frac{\partial M_{D}}{\partial y_{i}}\right)}{\sum_{D} M_{D}} = \begin{pmatrix} G_{M} \\ N \sum_{i} c_{iG} \left(\frac{\partial M_{B}}{\partial y_{i}} - x_{B} \sum_{D} \frac{\partial M_{D}}{\partial y_{i}}\right) \\ \sum_{D} M_{D} \end{pmatrix}$$

Box I.

Similar to Eq. (28), $\frac{dM_A^a}{dk_i}$ can be expressed as

$$\frac{dM_A^{\alpha}}{dk_i} = \sum_i \frac{\partial M_A^{\alpha}}{\partial y_i^{\alpha}} \frac{dy_i^{\alpha}}{dk_i}.$$
 (40)

where $\frac{\partial M_A^\alpha}{\partial k_j}=0$ and sublattice indices are omitted. Eq. (40) is then inserted into Eq. (39) to give

$$\frac{dN_A}{dk_j} = \sum_{\alpha} \frac{d\mathcal{N}^{\alpha}}{dk_j} M_A^{\alpha} + \sum_{\alpha} \mathcal{N}^{\alpha} \sum_{i} \frac{\partial M_A^{\alpha}}{\partial y_i^{\alpha}} \frac{dy_i^{\alpha}}{dk_j} = 0. \tag{41} \label{eq:41}$$

Lastly, when composition is specified as a condition, the total derivative of Eq. (6) with respect to k_j is derived and set equal to zero. With application of Eq. (40), this gives

$$\begin{split} \frac{dx_{A}}{dk_{j}} &= \\ &\underbrace{\sum_{\alpha} \frac{d\mathcal{N}^{\alpha}}{dk_{j}} M_{A}^{\alpha} + \sum_{\alpha} \mathcal{N}^{\alpha} \sum_{i} \frac{\partial M_{A}^{\alpha}}{\partial y_{i}^{\alpha}} \frac{dy_{i}^{\alpha}}{dk_{j}} - x_{A} \left(\sum_{\alpha} \frac{d\mathcal{N}^{\alpha}}{dk_{j}} \sum_{B} M_{B}^{\alpha} + \sum_{\alpha} \mathcal{N}^{\alpha} \sum_{B} \sum_{i} \frac{\partial M_{B}^{\alpha}}{\partial y_{B}^{\alpha}} \frac{dy_{i}^{\alpha}}{dk_{j}} \right)}_{\sum_{\alpha} \mathcal{N}^{\alpha} \sum_{B} M_{B}^{\alpha}} \end{split}$$

The conditions of the equilibrium calculation and the assignment of k_j produce the specific form of Eq. (34) that is inserted into Eqs. (41) and (42). Then, similar to the construction of the equilibrium matrix linear system, Eqs. (37), (41), and (42) are used to solve for $\frac{d\mathbf{W}}{dk_j}$. Finally, the calculated values of $\frac{d\mathbf{W}}{dk_j}$ are substituted into Eq. (34) to compute $\frac{dy_{is}^a}{dk_i}$. Two examples are given below.

4.2. Example: Jansson derivatives with respect to temperature

Assume a ternary A-B-C system with one stable phase in which temperature, pressure, amount of each component, and composition are conditions. Let x_C be the dependent composition variable, and assign $k_i = T$. Then Eqs. (21) and (34) take the below forms, respectively:

$$\Delta y_{is}^{\alpha} = c_{iG}^{\alpha} + \sum_{A} c_{iA}^{\alpha} \mu_{A},\tag{43}$$

$$\frac{dy_{is}^{\alpha}}{dT} = \frac{d\Delta y_{is}^{\alpha}}{dT} = c_{iT}^{\alpha} + \sum_{i} c_{iA}^{\alpha} \frac{d\mu_{A}}{dT}.$$
 (44)

To clarify, c_{iG}^{α} is an explicit function of T, and the partial derivative of c_{iG}^{α} with respect to T is c_{iT}^{α} . Inserting Eq. (44) into Eqs. (41) and (42) results in the linear system presented in Box II: Note that to recover the finite difference notation that Sundman et al. use in [7], start by representing the derivatives in the column vector on the left-hand side as ratios of finite differences. Then, multiply the whole system by ΔT ,

add another row and column to the matrix on the left-hand side to accommodate adding ΔT to the vector of values to be solved for, move all values that are now multiplied by ΔT from the right-hand side to the left-hand side, and set $\Delta T=1$. Thus, the two methods produce the same answer. However, the method proposed in this work removes a redundant equation from the linear system (the assignment $\Delta T=1$), which allows for the equilibrium matrix to be reused for the calculation of derivatives (see the equilibrium matrix in Eq. (31)). Since matrix inversion can be an expensive computation, avoiding the construction and inversion of a new matrix for these calculations can lead to greater computational efficiency.

4.3. Example: Jansson derivatives with respect to composition

Once again, assume a ternary A-B-C system with one stable phase in which temperature, pressure, amount of each component, and composition are conditions. Let x_C be the dependent composition variable, and assign $k_j = x_B$. Then, because Eq. (21) depends only on the conditions of the equilibrium calculation, Δy_{is}^{α} is once again given by Eq. (43). Conversely, Eq. (34) becomes

$$\frac{dy_{is}^{\alpha}}{dx_B} = \frac{d\Delta y_{is}^{\alpha}}{dx_B} = \sum_A c_{iA}^{\alpha} \frac{d\mu_A}{dx_B}.$$
 (46)

Note that the partial derivative of Δy_{is}^{α} with respect to x_B equals zero because all composition dependencies in these models are given as functions of **Y**, not **x**. Since composition is now changing, Eq. (42) is no longer set equal to zero for the derivatives of the independent composition variables. That is, for this system, $\frac{dx_B}{dx_B} = 1$ and the sum of $\frac{dx_A}{dx_B}$ and $\frac{dx_C}{dx_B}$ must equal -1. Setting $\frac{dx_A}{dx_B} = -\frac{1}{2}$ and inserting Eq. (46) into Eqs. (41) and (42) gives the linear system in Box III: As with the example in Section 4.2 where the derivative is taken with respect to a potential, the equilibrium matrix is recovered for the calculation of derivatives with respect to composition and requires only that a new column vector for the right-hand side be constructed.

4.4. Applied examples

For the two examples below and for those in Section 5.2, all phase diagrams are plotted using an in-development mapping module found in the PyCalphad GitHub repository under pull request #517 [19], and all Jansson derivatives are calculated using the PyCalphad development branch under pull request #432 [20]. All finite difference approximations are computed using the second-order central difference technique employed by NumPy's gradient function [21].

$$\begin{pmatrix}
M_{A} & M_{B} & M_{C} & 0 \\
\mathcal{N} \sum_{i} c_{iA} \sum_{D} \frac{\partial M_{D}}{\partial y_{i}} & \mathcal{N} \sum_{i} c_{iB} \sum_{D} \frac{\partial M_{D}}{\partial y_{i}} & \mathcal{N} \sum_{i} c_{iC} \sum_{D} \frac{\partial M_{D}}{\partial y_{i}} & \sum_{D} M_{D} \\
\frac{\sum_{i} c_{iA} \left(\frac{\partial M_{A}}{\partial y_{i}} - x_{A} \sum_{D} \frac{\partial M_{D}}{\partial y_{i}}\right) & \sum_{i} c_{iB} \left(\frac{\partial M_{A}}{\partial y_{i}} - x_{A} \sum_{D} \frac{\partial M_{D}}{\partial y_{i}}\right) & \sum_{i} c_{iC} \left(\frac{\partial M_{A}}{\partial y_{i}} - x_{A} \sum_{D} \frac{\partial M_{D}}{\partial y_{i}}\right) & \sum_{D} M_{D} & \frac{d_{A} - x_{A} \sum_{D} M_{D}}{\sum_{D} M_{D}} & \frac{d_{A} - x_{A} \sum_{D} d_{D}}{\sum_{D} d_{D}} & \frac{d_{A} - x_{A} \sum_{D} d_{D}}{d_{A} - x_{A} \sum_{D} d_{D}} & \frac{d_{A} - x_{A} \sum_{D} d_{D}}{d_{A} - x_{A} \sum_{D} d_{D}} & \frac{d_{A} - x_{A} \sum_{D} d_{D}}{d_{A} - x_{A} \sum_{D} d_{D}} & \frac{d_{A} - x_{A} \sum_{D} d_{D}}{d_{A} - x_{A} \sum_{D} d_{D}} & \frac{d_{A} - x_{A} \sum_{D} d_{D}}{d_{A} - x_{A} \sum_{D} d_{D}} & \frac{d_{A} - x_{A} \sum_{D} d_{D}}{d_{A} - x_{A} \sum_{D} d_{D}} & \frac{d_{A} - x_{A} \sum_{D} d_{D}}{d_{A} - x_{A} \sum_{D} d_{D}} & \frac{d_{A} - x_{A} \sum_{D} d_{D}}{d_{A} - x_{A} \sum_{D} d_{D}} & \frac{d_{A} - x_{A} \sum_{D} d_{D}}{d_{A} - x_{A} \sum_{D} d_{D}} & \frac{d_{A} - x_{A} \sum_{D} d_{D}}{d_{A} - x_{A} \sum_{D} d_{D}} & \frac{d_{A} - x_{A} \sum_{D} d_{D}}{d_{A} - x_{A} \sum_{D} d_{D}} & \frac{d_{A} - x_{A} \sum_{D} d_{D}}{d_{A} - x_{A} \sum_{D} d_{D}} & \frac{d_{A} - x_{A} \sum_{D} d_{D}}{d_{A} - x_{A} \sum_{D} d_{D}} & \frac{d_{A} - x_{A} \sum_{D} d_{D}}{d_{A} - x_{A} \sum_{D} d_{D}} & \frac{d_{A} - x_{A} \sum_{D}$$

Box II.

$$\begin{pmatrix}
M_{A} & M_{B} & M_{C} & 0 \\
\mathcal{N} \sum_{i} c_{iA} \sum_{D} \frac{\partial M_{D}}{\partial y_{i}} & \mathcal{N} \sum_{i} c_{iB} \sum_{D} \frac{\partial M_{D}}{\partial y_{i}} & \mathcal{N} \sum_{i} c_{iC} \sum_{D} \frac{\partial M_{D}}{\partial y_{i}} & \sum_{D} M_{D} \\
\frac{\sum_{i} c_{iA} \left(\frac{\partial M_{A}}{\partial y_{i}} - x_{A} \sum_{D} \frac{\partial M_{D}}{\partial y_{i}}\right) & \sum_{i} c_{iB} \left(\frac{\partial M_{A}}{\partial y_{i}} - x_{A} \sum_{D} \frac{\partial M_{D}}{\partial y_{i}}\right) & \sum_{i} c_{iC} \left(\frac{\partial M_{A}}{\partial y_{i}} - x_{A} \sum_{D} \frac{\partial M_{D}}{\partial y_{i}}\right) & \frac{M_{A} - x_{A} \sum_{D} M_{D}}{\mathcal{N} \sum_{D} M_{D}} \\
\frac{\sum_{i} c_{iA} \left(\frac{\partial M_{B}}{\partial y_{i}} - x_{B} \sum_{D} \frac{\partial M_{D}}{\partial y_{i}}\right) & \sum_{i} c_{iC} \left(\frac{\partial M_{B}}{\partial y_{i}} - x_{B} \sum_{D} \frac{\partial M_{D}}{\partial y_{i}}\right) & \frac{M_{A} - x_{A} \sum_{D} M_{D}}{\mathcal{N} \sum_{D} M_{D}} \end{pmatrix} \begin{pmatrix} \frac{d\mu_{A}}{dx_{B}} \\ \frac{d\mu_{B}}{dx_{B}} \\ \frac{d\mu_{C}}{dx_{B}} \\ \frac{d\mu_{C}}{dx_{B}} \end{pmatrix} \\
\frac{d\mu_{C}}{dx_{B}} \end{pmatrix}$$

$$\frac{\sum_{i} c_{iA} \left(\frac{\partial M_{B}}{\partial y_{i}} - x_{B} \sum_{D} \frac{\partial M_{D}}{\partial y_{i}}\right)}{\sum_{D} M_{D}} & \frac{\sum_{i} c_{iC} \left(\frac{\partial M_{B}}{\partial y_{i}} - x_{B} \sum_{D} \frac{\partial M_{D}}{\partial y_{i}}\right)}{\sum_{D} M_{D}} & \frac{M_{B} - x_{B} \sum_{D} M_{D}}{\mathcal{N} \sum_{D} M_{D}} \end{pmatrix} \begin{pmatrix} \frac{d\mu_{A}}{dx_{B}} \\ \frac{d\mu_{B}}{dx_{B}} \\ \frac{d\mu_{C}}{dx_{B}} \\ \frac{d\mu_{C}}{dx_{B}} \end{pmatrix}$$

$$\frac{d\mu_{C}}{dx_{B}} = \frac{1}{2} \begin{pmatrix} 0 \\ 0 \\ -\frac{1}{2} \\ 1 \end{pmatrix}$$

Box III.

4.4.1. Calculating heat capacity in the Al-Fe system

This example uses the thermodynamic description of the Al-Fe system provided in [22], and a phase diagram generated from this description is provided in Fig. 1. Recalling Section 2.2, in the context of equilibrium calculations, isobaric heat capacity is the *total* derivative of equilibrium enthalpy with respect to temperature while holding pressure and amounts of components constant:

$$C_p = \frac{dH}{dT} = \frac{\partial H}{\partial T} + \frac{\partial H}{\partial \mathcal{N}} \frac{d\mathcal{N}}{dT} + \frac{\partial H}{\partial \mathbf{Y}} \frac{d\mathbf{Y}}{dT}. \tag{48}$$

Equilibrium enthalpy of the system is calculated over the temperature interval [$1600-2000\ K$] at constant composition $x_{Al}=0.25$. These conditions were deliberately chosen to capture enthalpy and isobaric heat capacity through a phase change, which is the B2 phase melting to form the Liquid phase in this case. Following the same conditions, three methods are used to calculate the isobaric heat capacity: Jansson derivatives, partial derivatives of equilibrium enthalpy computing only the first term on the right-hand side of Eq. (48), and finite differences. The results are plotted in Fig. 2.

Fig. 2 shows that when only a single phase is stable, all three methods of calculating the constant pressure heat capacity agree well. However, for temperatures in which both the B2 and Liquid phases are stable, the Jansson derivative and finite difference methods predict a constant pressure heat capacity approximately two orders of magnitude higher than the partial derivative technique. This is because the partial derivative method does not account for latent heat contributions to the

heat capacity. Similarly, significant changes in constitution/ordering can lead to changes in configurational entropy which, if neglected, can also lead to large under-predictions of the heat capacity.

This example illustrates the danger of neglecting contributions to the heat capacity from dependent variables of the Gibbs energy minimization (i.e. neglecting the second and third terms on the right-hand side of Eq. (48)).

The calculation of the effective heat capacity across a phase change is important in a number of practical applications. For example, in the context of Additive Manufacturing (AM), the prediction of the characteristics of the melt pool as a function of process conditions is essential [23,24]. Thermal models that neglect accounting for the latent heat of melting (or boiling) tend to overestimate the temperature excursions within the melt pool, leading to significant discrepancies in the predicted melt pool characteristics relative to the ground truth [25, 26]. Most implementations of AM-relevant thermal models incorporate the effects of the latent heat by using a lumped capacitance approach—i.e. they assume a constant heat capacity that, when integrated over the coexistence temperature range equals the latent heat. A more thermodynamically-rigorous approach would avoid using these ad-hoc methods and instead rely on the formal definition of the heat capacity and its implementation through the Jansson derivative approach, as done in this section. Thermo-Calc's new Additive Manufacturing module implements this approach in the computation of effective thermo-physical properties needed for the calculations of the melting/solidification behavior.

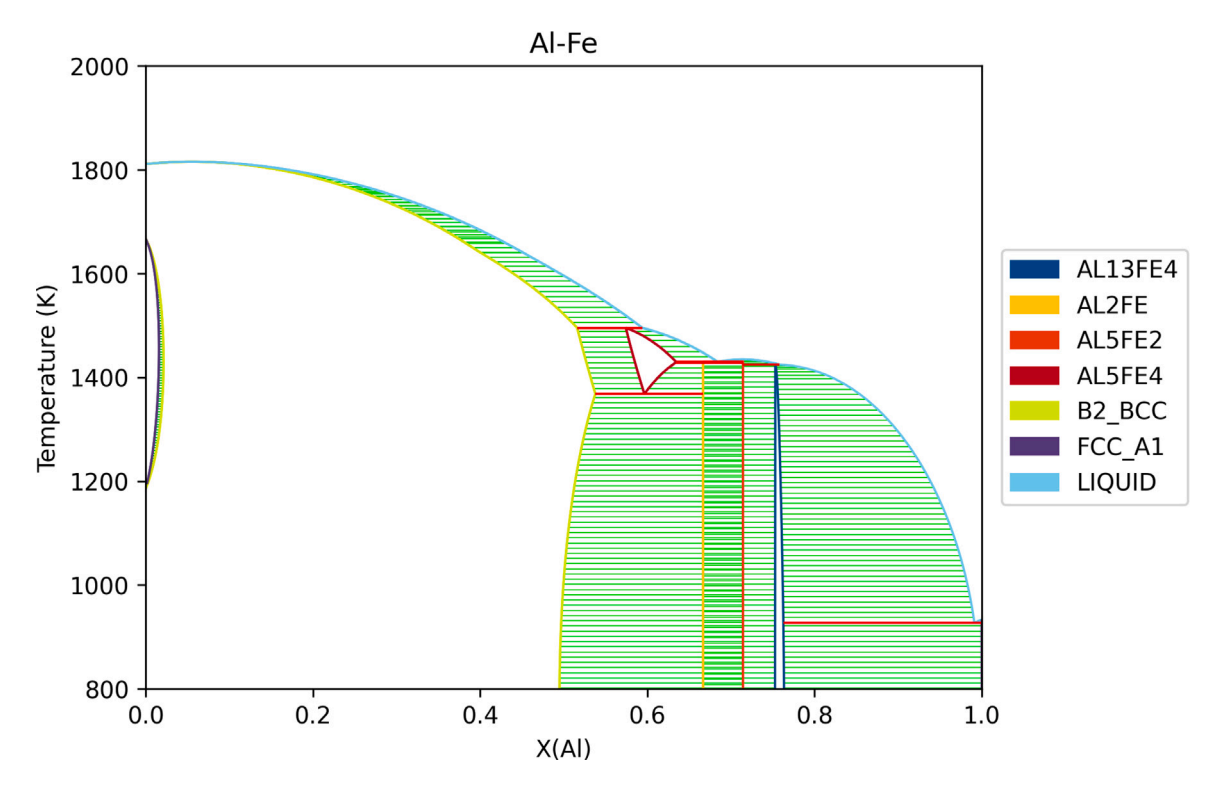


Fig. 1. Phase diagram of the Al-Fe system.

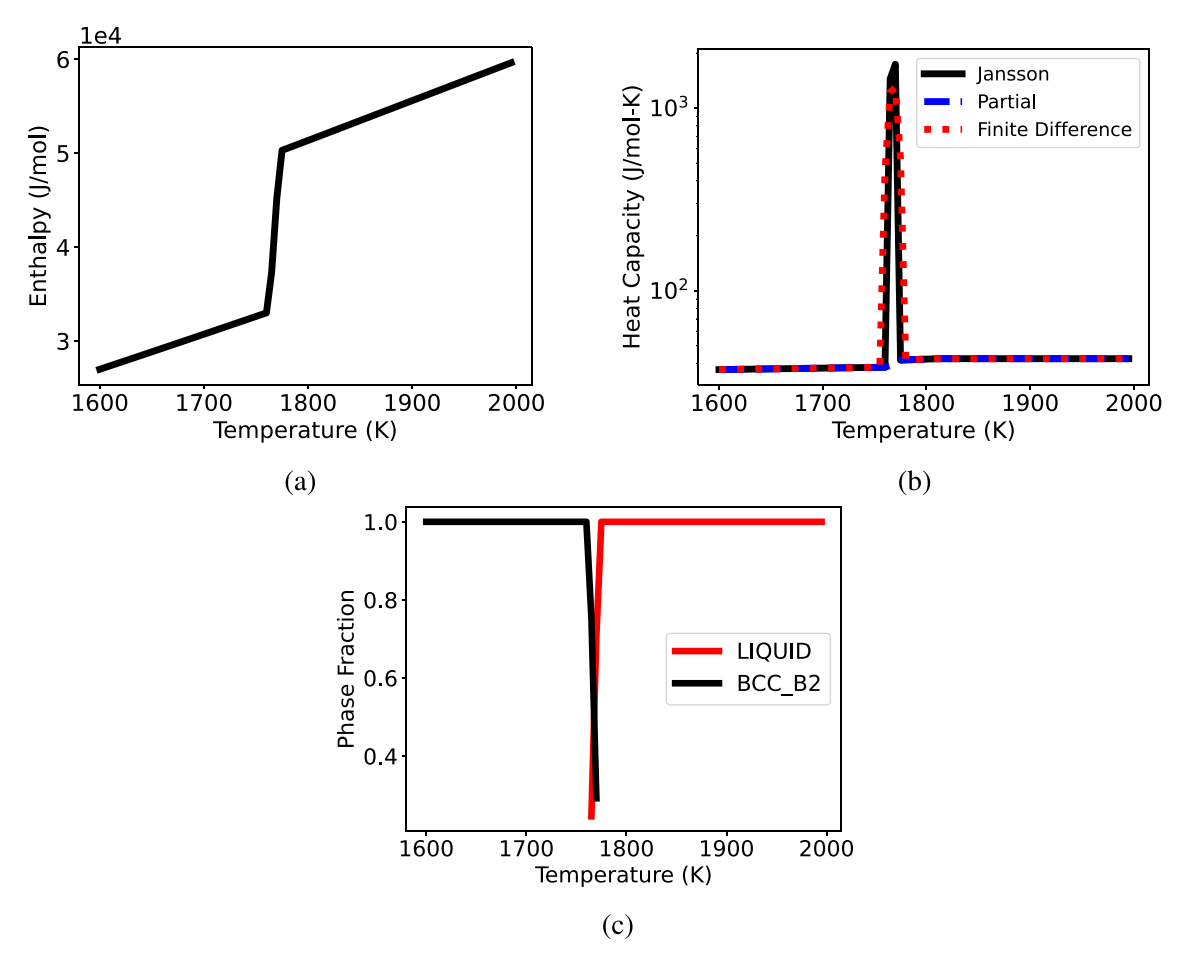


Fig. 2. (a) Equilibrium enthalpy, (b) Jansson derivative, partial derivative, and finite difference approximations of the constant pressure heat capacity, and (c) phase fractions all as functions of temperature for the Al-Fe system at $x_{AI} = 0.25$.

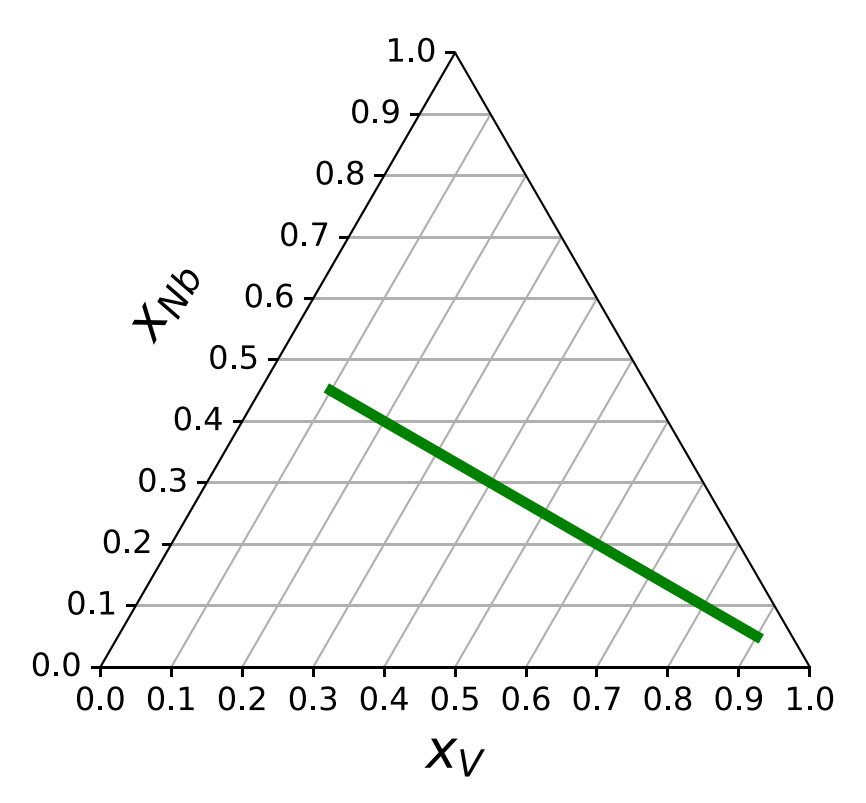


Fig. 3. Direction of single-phase equilibrium calculation composition conditions through composition space in the Nb-V-W system.

4.4.2. Calculating thermodynamic factors for the BCC phase in the Nb-V-W system

In this example, single-phase equilibrium calculations are used to calculate the chemical potentials of all components of the BCC phase in the Nb-V-W system along the direction in composition space displayed in Fig. 3. That is, starting at conditions $x_V=0.1$ and $x_{Nb}=x_W=0.45$ with x_W assigned as the dependent composition variable, x_{Nb} and x_W decrease symmetrically as x_V increases to $x_V=0.9$ while temperature is held at 1200 K. Adhering to the same conditions, thermodynamic factors of all three components with respect to x_V were calculated using Jansson derivatives and finite differences. In the Jansson derivative calculations, x_W is the dependent composition variable and $\frac{dx_{Nb}}{dx_V}$ was chosen to equal $-\frac{1}{2}$. Data for the thermodynamic description of the BCC phase for this system was generated in [27] and compiled into database format using [28].

The results are displayed in Fig. 4. For all calculated thermodynamic factors, the Jansson derivative and finite difference methods show excellent agreement.

The ability of Jansson derivatives to efficiently calculate analytic derivatives of chemical potential with respect to composition (and even temperature and pressure) could lead to more robust multi-physics-informed phase field and other mass transport simulations in which the driving force for transport relies on the spatial gradient of chemical potential. In a recent study [29], interdiffusion of U and Zr in U-Pu-Zr nuclear fuel rods was investigated by coupling the thermodynamic equilibrium calculation engine Thermochimica [30] with BISON [31], a nuclear fuel performance software used to model thermomechanics and mass transport. More specifically, BISON was used to solve the below diffusion equation using chemical potential and composition inputs calculated in Thermochimica:

$$\frac{\partial n_A}{\partial t} + \nabla \cdot \left(-\mathcal{M}_A n_A \nabla \mu_A \right) = 0 \tag{49}$$

where n_A is the volumetric density of component A, t is time, \mathcal{M}_A is the mobility of component A, and $\nabla \mu_A$ is the spatial gradient of the

chemical potential of component *A*. Applying the chain rule, $\nabla \mu_A$ can be further expressed as a function of x_A , T, and P:

$$\nabla \mu_A = \frac{d\mu_A}{dx_A} \nabla x_A + \frac{d\mu_A}{dT} \nabla T + \frac{d\mu_A}{dP} \nabla P. \tag{50}$$

As evidenced by Eqs. (49) and (50), injecting Jansson derivatives of chemical potential into the mass transport solver of such a multiphysics setup could facilitate more efficient and robust solutions of Eq. (49) because only the spatial gradients of x_A , T, and P would need to be solved for numerically.

5. Derivatives of residual driving force with respect to composition

The residual driving force—a measure of the distance between the Gibbs energy of a metastable phase and the current stable common tangent hyperplane—is a useful phase stability metric. This information, for example, could be used to inform a thermodynamic modeling optimizer as it navigates the parameter space in order to agree with experimental observations attesting to the presence (or absence) of a phase under specific thermodynamic conditions. In other cases, information about the residual driving force can be used to inform the exploration of high-dimensional composition spaces. For example, Galvan et al. [16] mapped the search over an alloy space in order to meet specific phase constitution constraints to the solution of a constraint satisfaction problem. In their setup, once a region was identified as meeting such phase constitution requirements, the now deemed feasible space was expanded through an active learning procedure. The framework, however, could only work once a feasible region had been identified in the first place. In general, all alloy search approaches that rely exclusively on the outcome of Gibbs minimization without accounting for changes in phase stability of metastable phases would have to first discover a feasible region in order to then expand the feasible space. This discovery process could be quite expensive and time-consuming if the feasible space is a small fraction of the total alloy design space.

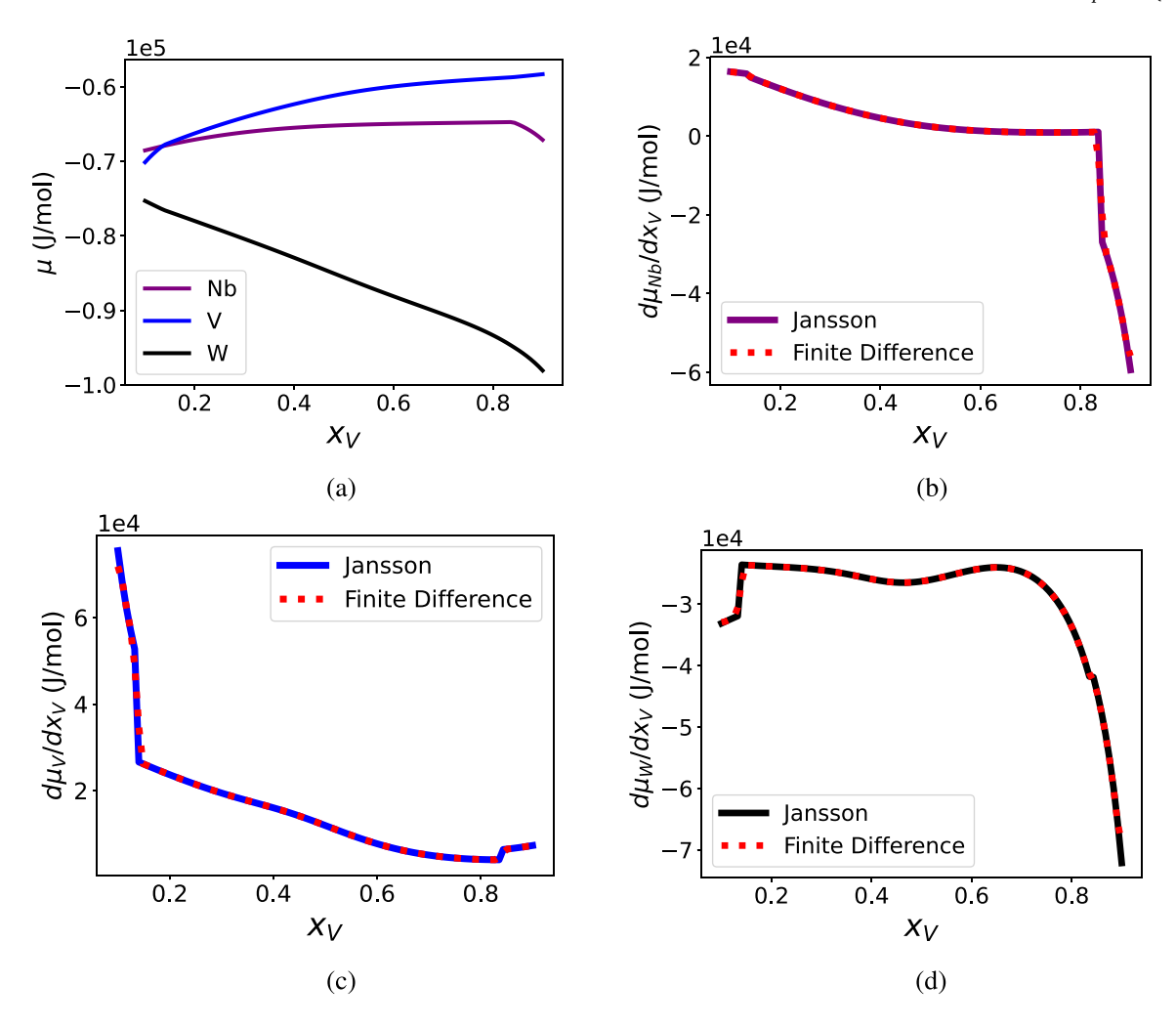


Fig. 4. (a) Chemical potentials of all components and Jansson derivative and finite difference approximations of (b) $\frac{d\mu_V}{dx_V}$, (c) $\frac{d\mu_{Nb}}{dx_V}$, and (d) $\frac{d\mu_W}{dx_V}$ where $\frac{dx_{Nb}}{dx_V} = \frac{dx_W}{dx_V} = -\frac{1}{2}$ for the BCC single phase equilibrium in the Nb-V-W system at 1200 K.

A much better approach would be to consider the residual driving force as a differentiable—and optimizable—quantity. Residual driving force derivatives with respect to composition would allow for the employment of gradient-based optimization tools, which have the potential to lower the computational cost associated with the targeted exploration of vast alloy spaces—e.g. the high entropy alloy space [17]—by several orders of magnitude. To this end, this section describes two different constructions of the residual driving force, derives gradients of these quantities with respect to overall system and individual phase compositions, and provides an example of calculating these gradients for residual driving forces of the B2 phase in the Ni-Ti system.

5.1. Formulation of residual driving force and its derivatives

Adopting the definition from [15], the residual driving force for phase α is given by

$$R^{\alpha} = G^{\alpha} - \sum_{i} \bar{\mu}_{A} x_{A}^{\alpha} \tag{51}$$

where $\bar{\mu}_A$ is the chemical potential of component A defining the target hyperplane, x_A^α is the composition of component A at the α phase vertex, and G^α is the single-phase, composition-constrained minimum Gibbs energy conditioned on the composition at the α phase vertex. In this work, two constructions of the target hyperplane are considered, and the derivatives of their corresponding residual driving forces with

respect to overall system composition and individual phase vertex compositions are discussed below.

5.1.1. Constructing the target hyperplane from a measured overall composition

Let $\tilde{x}_A \in \tilde{\mathbf{x}}$ denote the measured overall system mole fraction of component A and $\tilde{x}_A^\alpha \in \tilde{\mathbf{x}}^\alpha$ denote the measured mole fraction of component A for the α phase vertex at equilibrium. For this case, the target hyperplane is defined by a multiphase equilibrium calculation at the measured overall system composition:

$$\bar{\mu}_A = \mu_A \tag{52}$$

where μ_A with no symbol above it signifies the chemical potential of component A for the multiphase equilibrium conditioned on $\tilde{\mathbf{x}}$.

In contrast, G^{α} is determined from a single phase equilibrium calculation conditioned on $\tilde{\mathbf{x}}^{\alpha}$. To denote that G^{α} is being calculated from a different equilibrium than the chemical potentials for the target hyperplane, any value arising from a single phase equilibrium conditioned on the corresponding phase vertex composition will be denoted with a "hat" (e.g. \hat{G}^{α}). Thus, Eq. (51) takes the form

$$R^{\alpha}(\mathbf{x}, \mathbf{x}^{\alpha}) = \hat{G}^{\alpha}(\mathbf{x}^{\alpha}) - \sum_{A} \mu_{A}(\mathbf{x})\hat{x}_{A}^{\alpha}, \tag{53}$$

where the dependence of each quantity on overall and vertex compositions is emphasized. Fig. 5 provides a visual representation of the terms in Eq. (53).

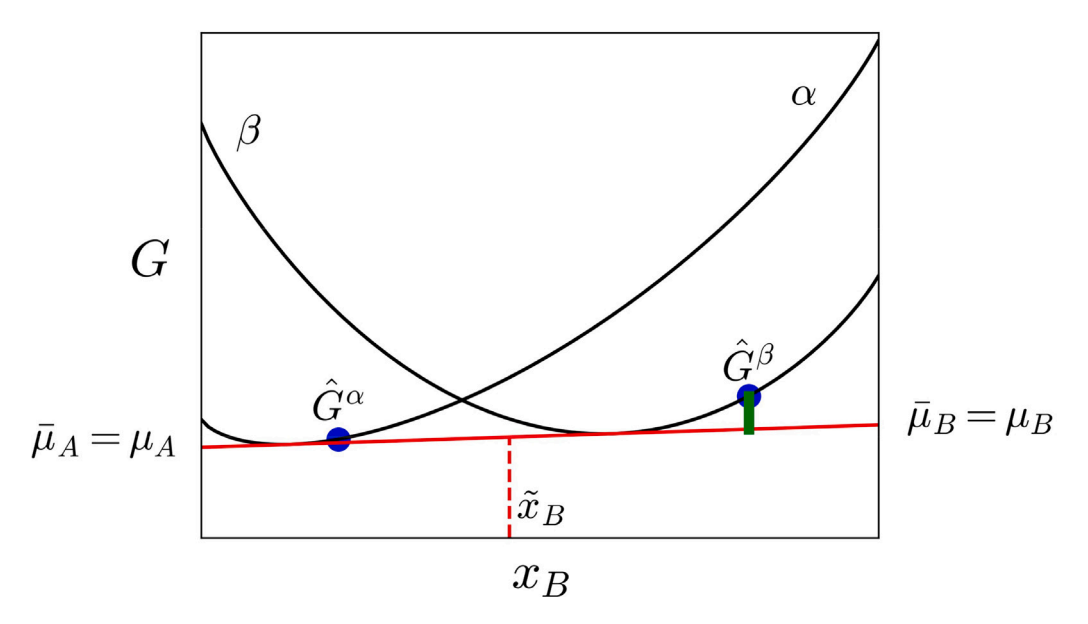


Fig. 5. Schematic of mean hyperplane and residual driving force when the measured overall composition is available. The residual driving force is given by the vertical distance between \hat{G} and the target hyperplane (green line).

Taking the total derivative of R^{α} with respect to x_A and holding vertex compositions constant gives

$$\frac{dR^{\alpha}}{dx_{A}} = \frac{d\hat{G}^{\alpha}}{dx_{A}} - \sum_{B} \frac{d\mu_{B}}{dx_{A}} \hat{x}_{B}^{\alpha} - \sum_{B} \mu_{B} \frac{d\hat{x}_{B}^{\alpha}}{dx_{A}} = -\sum_{B} \frac{d\mu_{B}}{dx_{A}} \hat{x}_{B}^{\alpha}, \tag{54}$$

where all $\frac{d\mu_B}{dx_A}$ are calculated from taking the Jansson derivative of the multiphase equilibrium calculation conditioned on the measured overall system composition with respect to x_A . Because vertex compositions are being held constant, all derivatives of phase vertex mole fractions and derivatives of values that are only functions of these compositions with respect to x_A in Eq. (54) equal zero.

Now, taking the derivative of R^{α} with respect to x_A^{α} and holding overall system composition and other vertex compositions constant gives

$$\frac{dR^{\alpha}}{dx_{A}^{\alpha}} = \frac{d\hat{G}^{\alpha}}{dx_{A}^{\alpha}} - \sum_{B} \frac{d\mu_{B}}{dx_{A}^{\alpha}} \hat{x}_{B}^{\alpha} - \sum_{B} \mu_{B} \frac{d\hat{x}_{B}^{\alpha}}{dx_{A}^{\alpha}} = \frac{d\hat{G}^{\alpha}}{dx_{A}^{\alpha}} - \sum_{B} \mu_{B} \frac{d\hat{x}_{B}^{\alpha}}{dx_{A}^{\alpha}}$$
(55)

where the derivative $\frac{d\hat{G}^{\alpha}}{dx_{B}^{\alpha}}$ is calculated from taking the Jansson derivative of the single phase equilibrium calculation conditioned on the measured α phase vertex composition with respect to x_{A} . All derivatives of overall system mole fractions and derivatives of values that are only functions of these compositions with respect to x_{A}^{α} equal zero since the overall system composition is held constant. The values of $\frac{d\hat{x}_{B}^{\alpha}}{dx_{A}^{\alpha}}$ depend on the assignments in the Jansson derivative calculation of the single phase equilibrium calculation conditioned on \tilde{x}^{α} . That is, $\frac{d\hat{x}_{A}^{\alpha}}{dx_{A}^{\alpha}}=1$, and the derivatives of the remaining α phase mole fractions with respect to x_{A}^{α} sum to -1 just as in the Jansson derivative calculation (see Section 4.3).

Inspection of Eq. (53) reveals that no terms are a function of any vertex compositions of other phases. Thus, for phase $\beta \neq \alpha$, the derivative of R^{α} with respect to x_A^{β} while holding overall system and other vertex compositions constant equals zero.

5.1.2. Constructing the target hyperplane from measured vertex compositions

Let $\tilde{x}^{\alpha}_{A} \in \tilde{\mathbf{x}}^{\alpha}$ denote the measured mole fraction of component A for the α phase vertex at equilibrium. For this case, there is no measured overall system composition. Thus, the target hyperplane is defined by an average of chemical potentials from multiphase equilibrium

calculations conditioned on the phase vertex compositions:

$$\bar{\mu}_A = \frac{1}{p} \sum_{\alpha} \mathring{\mu}_A^{\alpha} \tag{56}$$

where p is the number of measured stable phases at equilibrium and $\hat{\mu}_A^a$ denotes the chemical potential of component A from the multiphase equilibrium conditioned on $\tilde{\mathbf{x}}^a$. Similar to the "hat", the "ring" denotes a value from a multiphase equilibrium conditioned on a phase vertex composition. Thus, Eq. (51) takes the form

$$R^{\alpha}(\mathbf{x}^{\alpha}, \mathbf{x}^{\beta}, \dots) = \hat{G}^{\alpha}(\mathbf{x}^{\alpha}) - \sum_{l} \frac{\mathring{x}_{A}^{\alpha}}{p} \sum_{\mathbf{x}} \mathring{\mu}_{A}^{\gamma}(\mathbf{x}^{\gamma})$$
 (57)

where the dependence of each quantity on vertex compositions is emphasized. Note that \mathring{x}_A^α could also have a "hat" over it since both the multiphase α vertex and the single phase equilibrium calculations are conditioned on the same composition. Fig. 6 provides a visual representation of the terms in Eq. (57).

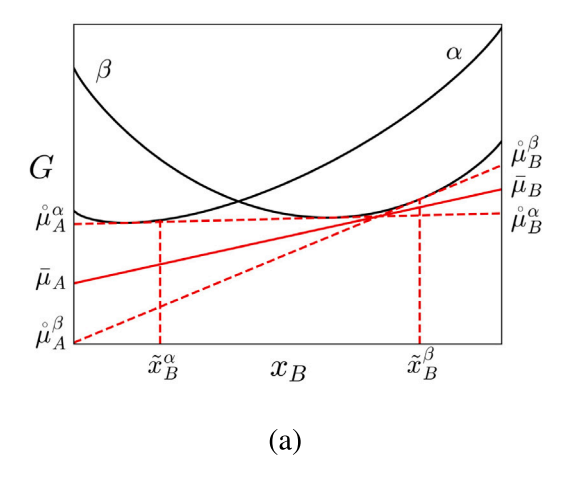
Inspection of Eq. (57) reveals that no terms are a function of overall system composition. Thus, the derivative of R^{α} with respect to x_A while holding all vertex compositions constant equals zero. Conversely, taking the derivative of R^{α} with respect to x_A^{α} and holding overall composition and other vertex compositions constant gives

$$\frac{dR^{\alpha}}{dx_{A}^{\alpha}} = \frac{d\hat{G}^{\alpha}}{dx_{A}^{\alpha}} - \sum_{B} \frac{\mathring{x}_{B}^{\alpha}}{p} \sum_{\beta} \frac{d\mathring{\mu}_{B}^{\beta}}{dx_{A}^{\alpha}} - \frac{1}{p} \sum_{B} \frac{d\mathring{x}_{B}^{\alpha}}{dx_{A}^{\alpha}} \sum_{\beta} \mathring{\mu}_{B}^{\beta}$$

$$= \frac{d\hat{G}^{\alpha}}{dx_{A}^{\alpha}} - \sum_{B} \frac{\mathring{x}_{B}^{\alpha}}{p} \frac{d\mathring{\mu}_{B}^{\alpha}}{dx_{A}^{\alpha}} - \sum_{B} \frac{d\mathring{x}_{B}^{\alpha}}{dx_{A}^{\alpha}} \ddot{\mu}_{B}$$
(58)

where all $\frac{d\mu_B^\alpha}{dx_A^\alpha}$ are calculated from taking the Jansson derivative of the multiphase equilibrium calculation conditioned on \mathbf{x}^α with respect to x_A . All derivatives of vertex mole fractions other than for phase α and derivatives of values that are only functions of these compositions with respect to x_A^α equal zero since the other vertex compositions are held constant. Similar to Eq. (55), the values of $\frac{d\tilde{x}_A^\alpha}{dx_A^\alpha}$ depend on the assignments in the Jansson derivative calculation of the multiphase equilibrium calculation conditioned on $\tilde{\mathbf{x}}^\alpha$.

Further inspection of Eq. (57) reveals that R^{α} is a function of the vertex compositions of other phases. Taking the derivative of R^{α} with respect to x^{β}_{A} and holding overall composition and other vertex



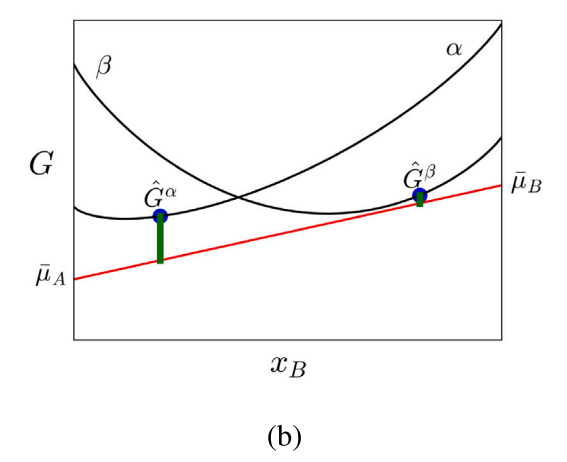


Fig. 6. Schematic of mean hyperplane and residual driving force when measured overall composition is unavailable. The target hyperplane is built in (a), and the residual driving force is given by the vertical distance between \hat{G} and the target hyperplane (green line) in (b).

compositions constant gives

$$\frac{dR^{\alpha}}{dx_{A}^{\beta}} = \frac{d\hat{G}^{\alpha}}{dx_{A}^{\beta}} - \sum_{B} \frac{\mathring{x}_{B}^{\alpha}}{p} \sum_{\gamma} \frac{d\mathring{\mu}_{B}^{\gamma}}{dx_{A}^{\beta}} - \frac{1}{p} \sum_{B} \frac{d\mathring{x}_{B}^{\alpha}}{dx_{A}^{\beta}} \sum_{\gamma} \mathring{\mu}_{B}^{\gamma} = -\sum_{B} \frac{\mathring{x}_{B}^{\alpha}}{p} \frac{d\mathring{\mu}_{B}^{\beta}}{dx_{A}^{\beta}}$$
(59)

where all $\frac{d\hat{\mu}_{B}^{\rho}}{dx_{A}^{\rho}}$ come from Jansson derivatives of the multiphase equilibrium calculation conditioned on $\tilde{\mathbf{x}}^{\rho}$, and many derivatives equal zero for the same reasons as in Eq. (58).

While two examples are presented here, it should be noted that the target hyperplane can be constructed in whatever fashion is convenient for the problem at hand. Once the target hyperplane is defined, the key to calculating the derivative of the residual driving force of a given phase with respect to the overall or a specific phase vertex composition is a matter of determining which composition each quantity is conditioned on. If a quantity comes from an equilibrium calculation not conditioned on the composition corresponding to the derivative, the derivative of that term is zero.

5.2. Example: Application to the Ni-Ti system

This case study leverages the thermodynamic description of the Ni-Ti system provided in [32]. The phase diagram of this system is provided Fig. 7. In this example, stability of the B2 phase is investigated at 1500 K near the B2/Liquid two-phase region with simulated measurements of $\tilde{x}_{Ti}=0.45, \, \tilde{x}_{Ti}^{B2}=0.47, \, \text{and} \, \, \tilde{x}_{Ti}^{L}=0.41.$ Derivatives of residual driving force are calculated for both constructions of the target hyperplane described above.

5.2.1. Constructing the target hyperplane from a measured overall composition

Fig. 8 displays R^{B2} as defined in Eq. (53) and the Jansson derivative of R^{B2} with respect to x_{Ti} as defined in Eq. (54) as functions of x_{Ti} in which the target hyperplane is constructed from a multiphase equilibrium calculation conditioned on x_{Ti} . For these calculations, x_{Ti}^{B2} and x_{Ti}^{L} are held at the assigned values given above while x_{Ti} varies along the interval [0.40, 0.50], which is centered on the assigned value $\tilde{x}_{Ti} = 0.45$. For this case, there is good agreement between the Jansson derivative and finite difference approximations. The equilibrium phase fractions as a function of x_{Ti} are also shown. Corners in the driving force plot and resulting discontinuities in the derivative correspond to changes in the set of stable phases. In this case, the sudden addition or subtraction of a stable phase can cause discontinuities in the derivative of the chemical potentials defining the target hyperplane, leading to the behavior seen here.

Fig. 9 displays R^{B2} still defined by Eq. (53) but shows the Jansson derivative with respect to x_{Ti}^{B2} as defined in Eq. (55). Both quantities are functions of x_{Ti}^{B2} and the target hyperplane is once again constructed from a multiphase equilibrium calculation conditioned on x_{Ti} . In contrast to the previous example, in these calculations x_{Ti} and x_{Ti}^{L} are held at the assigned values given above while x_{Ti}^{B2} varies along the interval [0.42, 0.52], which is centered on the assigned value $\tilde{x}_{Ti}^{B2} = 0.47$. For this case, the Jansson derivative and the finite difference approximation show excellent agreement, and there are no sharp corners in the residual driving force or visibly noticeable discontinuities in the derivative. This is because the target hyperplane is not a function of x_{Ti}^{B2} , so the chemical potentials defining it stay constant. Additionally, the single-phase composition-constrained equilibrium defining G^{B2} does not experience any changes of phase or rapid changes in internal ordering, which also contributes to the smoothness of the driving force curve.

5.2.2. Constructing the target hyperplane from measured vertex compositions

Fig. 10 displays \mathbb{R}^{B2} as defined in Eq. (57) and the Jansson derivative of R^{B2} with respect to x_{Ti}^{B2} as defined in Eq. (58) as functions of x_{Ti}^{B2} in which the target hyperplane is constructed from an average of multiphase equilibrium calculations conditioned on \boldsymbol{x}_{Ti}^{B2} and \boldsymbol{x}_{Ti}^{L} . Similar to the previous example, in these calculations x_{Ti} and x_{Ti}^L are held at \tilde{x}_{Ti} and \tilde{x}_{Ti}^L , respectively while x_{Ti}^{B2} varies along the interval [0.42, 0.52]. The equilibrium phase fractions as a function of the equilibrium conditioned on $x_{T_i}^{B2}$ are also shown. In this case, the Jansson derivative and finite difference approximation show great agreement, and while there is no noticeable corner in the driving force plot, there is a slight kink in the Jansson derivative plot near $x_{Ti}^{B2} = 0.476$ corresponding to the change in the set of stable phases. Interestingly, there is no noticeable corner in the driving force plot or kink in the Jansson derivative curve when the Liquid phase becomes stable again near $x_{Ti}^{B2} = 0.501$. Thus, while the removal of the Liquid phase from the set of stable phases causes a discontinuity in the chemical potentials from the B2 phase vertex, the effect on the overall derivative is lessened through averaging with the chemical potentials from the Liquid vertex equilibrium calculation, and the re-addition of this phase to the set of stable phases does not have to result in a discontinuity in the derivative.

Lastly, Fig. 11 displays R^{B2} as defined by Eq. (57) but shows the Jansson derivative with respect to x_{Ti}^L as defined in Eq. (59). Both quantities are functions of x_{Ti}^L and the target hyperplane is once again constructed from an average of multiphase equilibrium calculations conditioned on x_{Ti}^{B2} and x_{Ti}^L . In contrast to the previous example, in

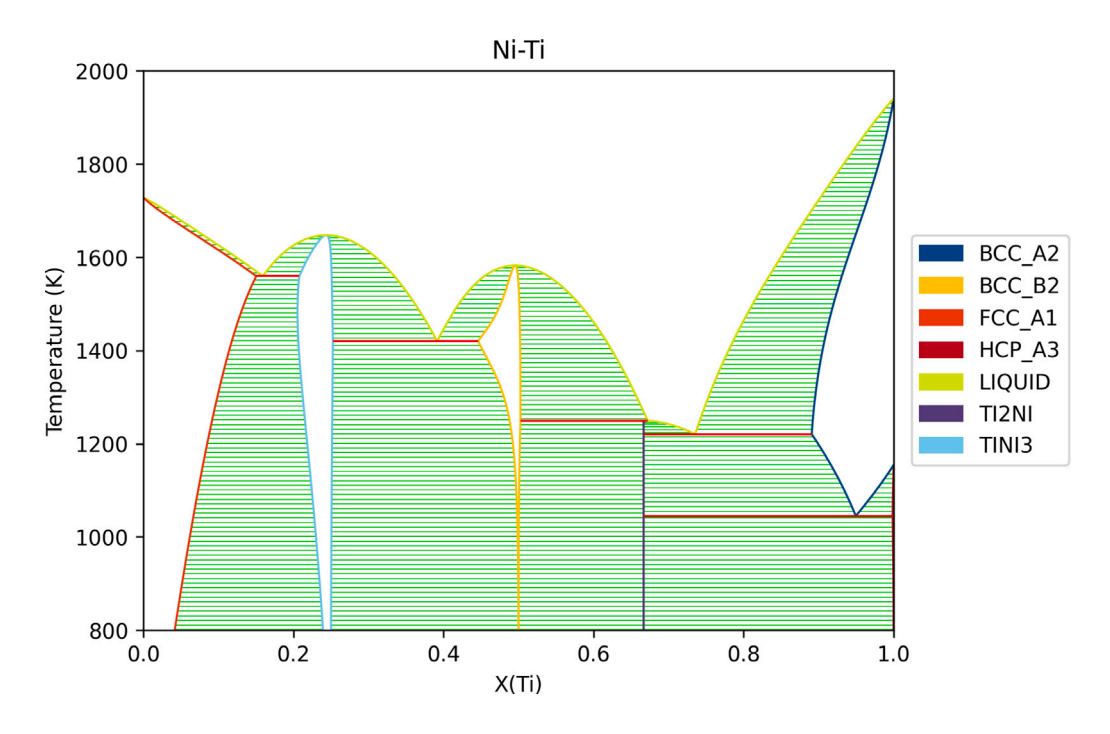


Fig. 7. Phase diagram of the Ni-Ti system.

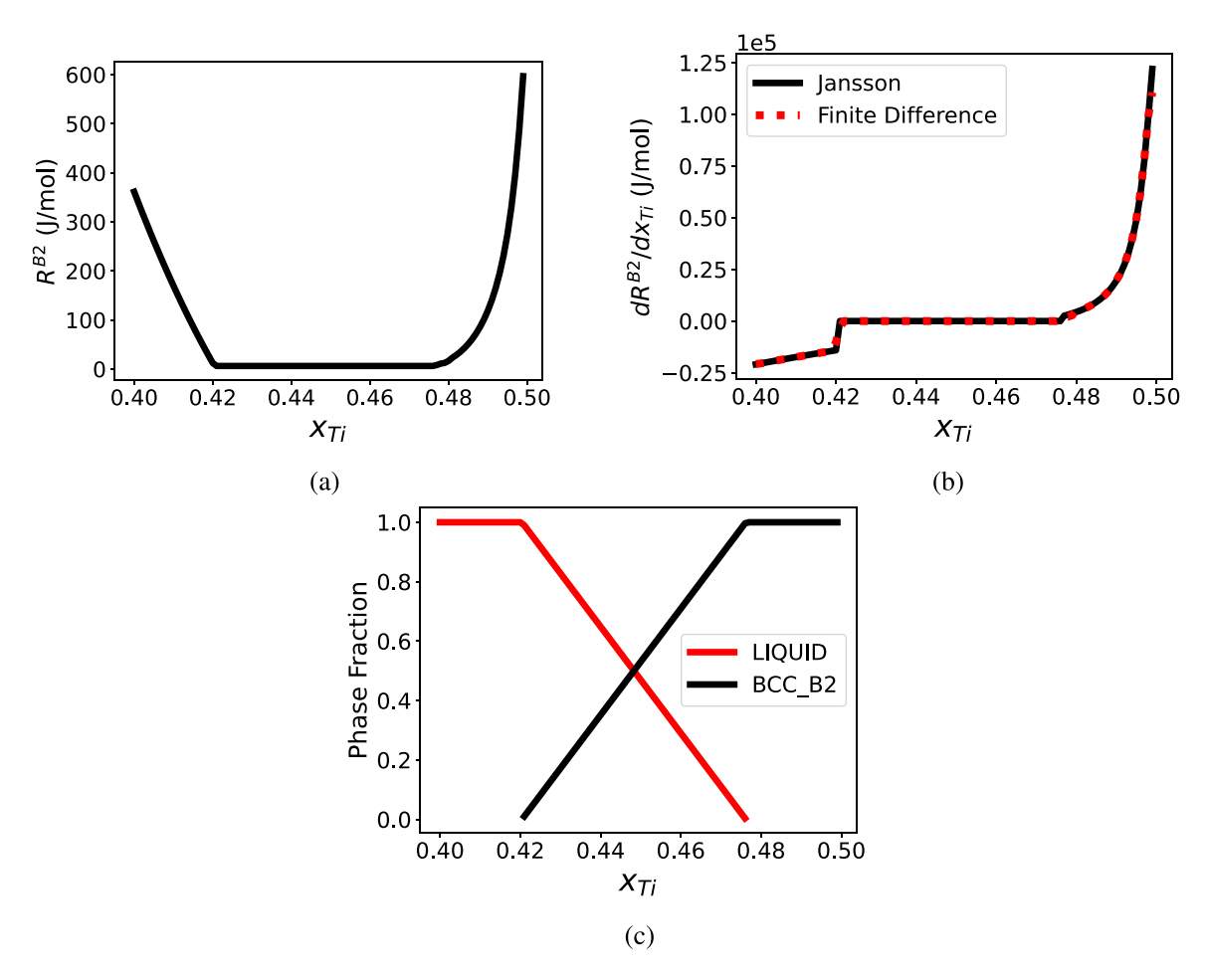


Fig. 8. (a) Residual driving force of the B2 phase R^{B2} , (b) Jansson derivative and finite difference approximation of the derivative of R^{B2} with respect to x_{Ti} , and (c) equilibrium phase fractions all as functions of x_{Ti} where the target hyperplane is constructed from a multiphase equilibrium calculation conditioned on x_{Ti} .

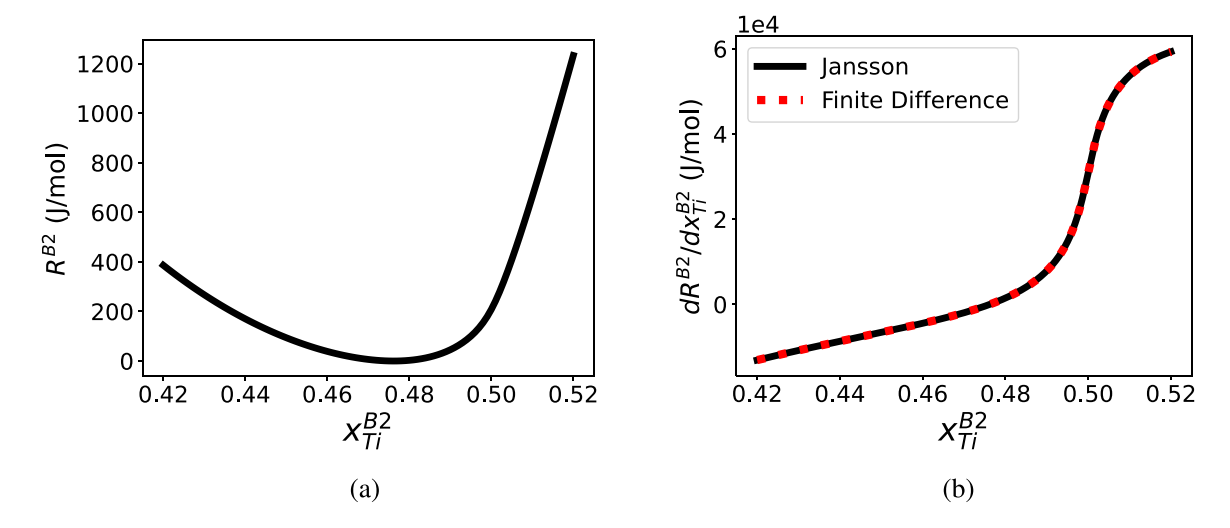


Fig. 9. (a) Residual driving force of the B2 phase R^{B2} and (b) Jansson derivative and finite difference approximation of the derivative of R^{B2} with respect to x_{Ti}^{B2} all as functions of x_{Ti}^{B2} where the target hyperplane is constructed from a multiphase equilibrium calculation conditioned on x_{Ti} .

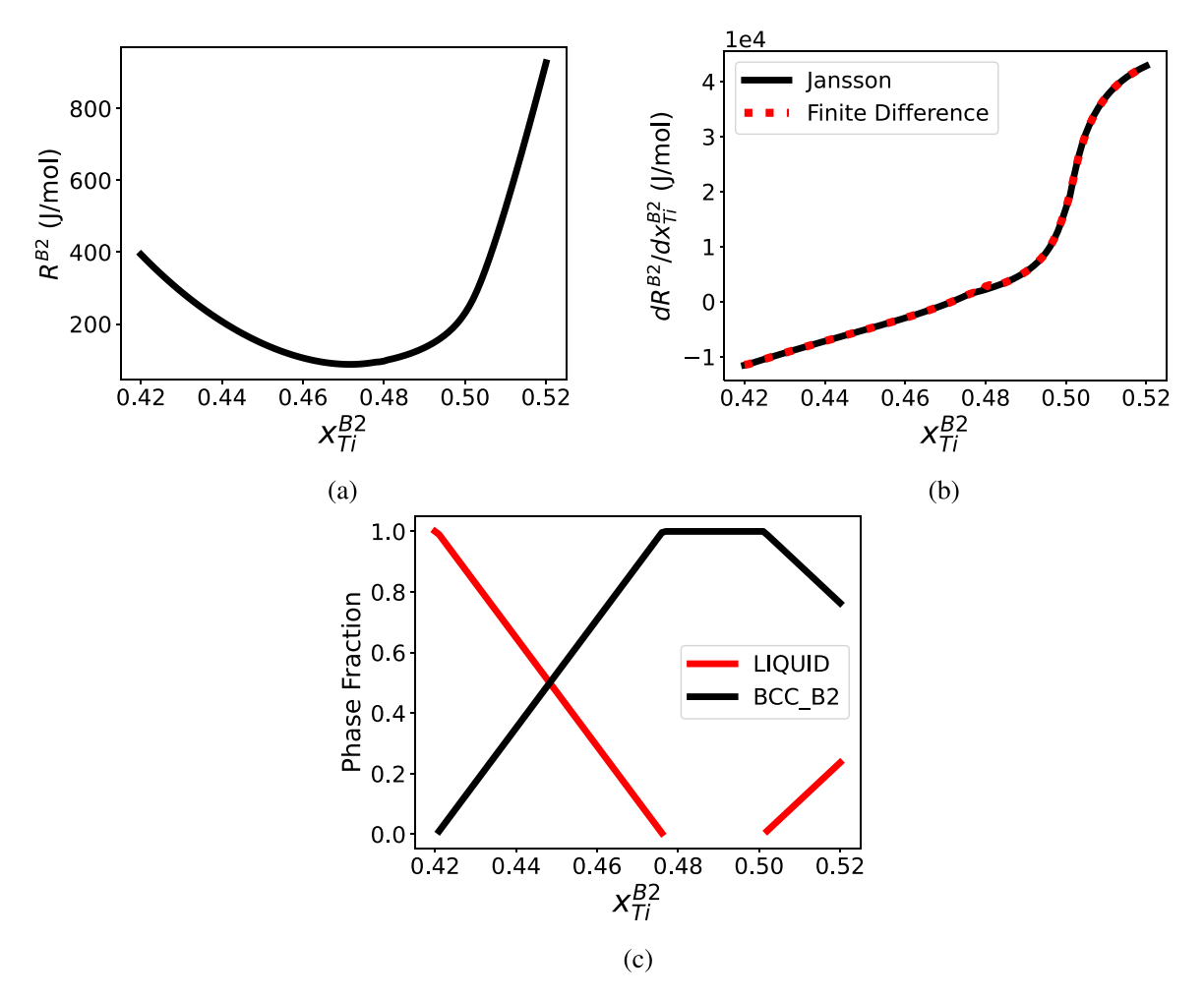


Fig. 10. (a) Residual driving force of the B2 phase R^{B2} , (b) Jansson derivative and finite difference approximation of the derivative of R^{B2} with respect to $x_{T_i}^{B2}$, and (c) equilibrium phase fractions all as functions of $x_{T_i}^{B2}$ where the target hyperplane is constructed from an average of multiphase equilibrium calculations conditioned on $x_{T_i}^{B2}$ and $x_{T_i}^{L}$.

these calculations x_{Ti} and x_{Ti}^{B2} are held at \tilde{x}_{Ti} and \tilde{x}_{Ti}^{B2} , respectively while x_{Ti}^{L} varies along the interval [0.36, 0.46] centered on the assigned value $\tilde{x}_{Ti}^{L}=0.41$. The equilibrium phase fractions as a function of

the equilibrium conditioned on x_{Ti}^L are also shown. For this case, the Jansson derivative and finite difference approximation once again agree quite well, and corners in the driving force curve and resulting

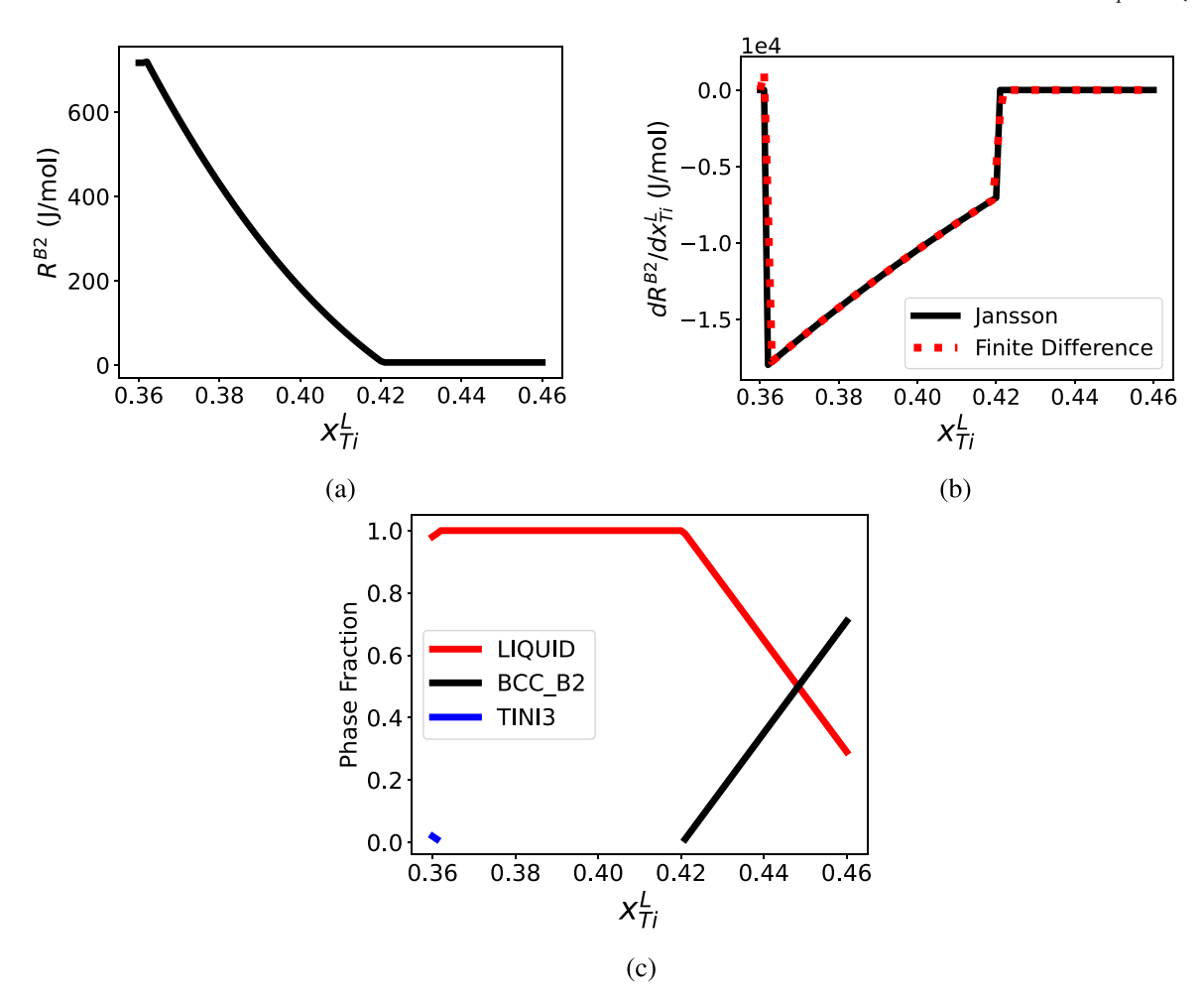


Fig. 11. (a) Residual driving force of the B2 phase R^{B2} , (b) Jansson derivative and finite difference approximation of the derivative of R^{B2} with respect to $x_{T_i}^L$, and (c) equilibrium phase fractions all as functions of $x_{T_i}^L$ where the target hyperplane is constructed from an average of multiphase equilibrium calculations conditioned on $x_{T_i}^{B2}$ and $x_{T_i}^L$.

discontinuities in the Jansson derivative correspond to changes in the set of stable phases.

5.2.3. Efficiency and robustness of Jansson derivatives versus numerical approximations

This case study concludes with a brief discussion about the advantages of calculating derivatives at equilibrium using Jansson derivatives as opposed to numerical methods. Throughout the applied examples in Sections 4 and 5, Jansson derivative and finite difference approximations show great agreement, even at discontinuities in the derivative. This is because the step size of the numerical approximation was able to be calibrated against the ground truth analytic values from Jansson derivatives. Fig. 12 extends the composition interval from the example displayed in Fig. 8 to capture another change in the set of stable phases and displays the ability of both methods to provide accurate point calculations and linear interpolations of the residual driving force derivative over a continuous composition interval with varying step size h. Because Jansson derivatives provide point queries of the analytic derivative using only the information from an equilibrium calculation at that point, all point calculations with this method are accurate, regardless of the step size. Furthermore, the linear interpolation from the Jansson derivative method converges rapidly, showing little change with increasing step size after h = 0.01. In contrast, the finite difference method provides fairly accurate point calculations and linear interpolations for the derivative for high values of h where the residual driving force is sufficiently smooth, but it does not fully capture the behavior of the derivative at higher values of x_{Ti} until a step size of

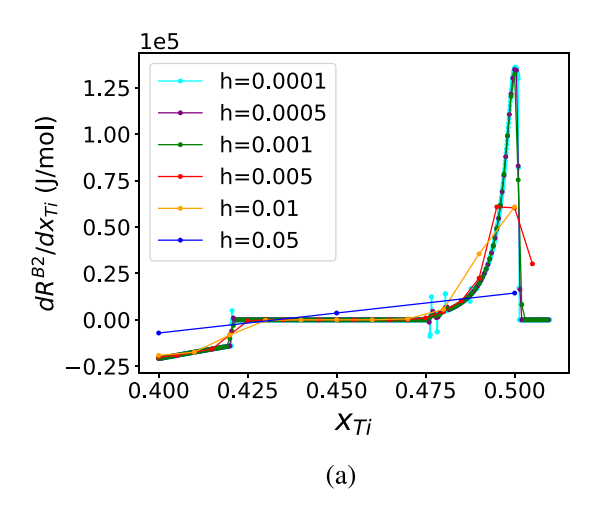
h=0.001. Moreover, as step size continues to decrease, the finite difference approach starts to diverge at discontinuities. While it may be possible to mitigate the instability with respect to step size in numerical derivatives through, e.g., an adaptive step size or change-of-variables approach, the use of Jansson derivatives makes that unnecessary.

This simple example illustrates that numerical derivatives can be of similar reliability and computational cost to Jansson derivatives when the differentiated quantity is sufficiently smooth with respect to the ordinate of interest and when there is adequate information to calibrate the step size. However, even when these conditions do not hold, Jansson derivatives provide a robust and efficient method of calculating derivatives at equilibrium.

6. Conclusions and future work

After 40 years of implementation, the mathematical justification for the Jansson derivative technique coupling to the widely-used SQP Lagrange-Newton minimizer for equilibrium calculations is rigorously described. As demonstrated, Jansson derivatives are vital for capturing contributions to the total derivative at equilibrium from dependent variables of the Gibbs energy minimization, such as phase internal degrees of freedom. Furthermore, this work demonstrates that, with the application of Jansson derivatives, the residual driving force of a phase can be applied as a differentiable metric for phase stability, allowing for gradient-based explorations of high-dimensional composition spaces.

Looking ahead, further application of the mathematical arguments presented in this work could lead to the derivation of methods for



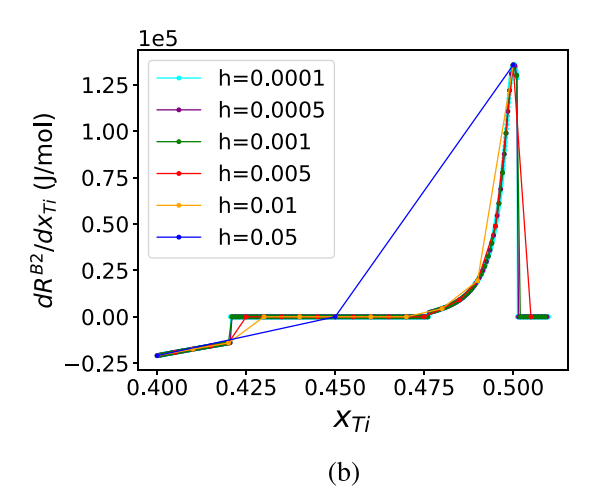


Fig. 12. (a) Finite difference and (b) Jansson derivative interpolations of the continuous derivative R^{B2} with respect to x_{Ti} with varying step size h.

calculating higher-order derivatives at equilibrium. Of specific interest, second derivatives with respect to model parameters could provide information matrices for maximum likelihood statistical analyses, and second derivatives with respect to composition would greatly aid the search for spinodal regions in complex multicomponent systems, which would be a key tool for the design of stable microstructures with superior properties [33,34].

CRediT authorship contribution statement

Courtney Kunselman: Writing – review & editing, Writing – original draft, Visualization, Methodology, Investigation, Formal analysis, Conceptualization. Brandon Bocklund: Visualization, Conceptualization. Axel van de Walle: Writing – review & editing, Resources. Richard Otis: Writing – review & editing, Methodology, Formal analysis, Conceptualization. Raymundo Arróyave: Writing – review & editing, Writing – original draft, Supervision, Methodology, Formal analysis, Conceptualization.

Declaration of competing interest

The authors declare that they have no known competing financial interests or personal relationships that could have appeared to influence the work reported in this paper.

Data availability

Code and databases for reproducing results are included as supplementary material.

Acknowledgments

Work at Lawrence Livermore National Laboratory (LLNL) was performed under the auspices of the U.S. Department of Energy by LLNL under Contract No. DE- AC52-07NA27344. Part of this research was carried out at the Jet Propulsion Laboratory, California Institute of Technology, under a contract with the National Aeronautics and Space Administration (80NM0018D0004). Useful discussions with Alicia Zhang in the initial development of this work are acknowledged. Partial support from the Caltech/JPL Innovative Software Initiative program is acknowledged. RA also wishes to acknowledge the support from NSF through Grant No. NSF-DMREF-2119103.

Appendix A

Without loss of generality, consider the derivative of G with respect to T while holding P constant and assume a closed system (the same

argument will work for taking the derivative with respect to P while holding T constant). Starting with Eq. (2), the differential of G takes the form

$$dG = \sum_{\alpha} d\mathcal{N}^{\alpha} G_{M}^{\alpha} + \sum_{\alpha} \mathcal{N}^{\alpha} dG_{M}^{\alpha} = \sum_{\alpha} d\mathcal{N}^{\alpha} G_{M}^{\alpha}$$
$$+ \sum_{\alpha} \mathcal{N}^{\alpha} \left(\frac{\partial G_{M}^{\alpha}}{\partial T} dT + \sum_{i} \frac{\partial G_{M}^{\alpha}}{\partial y_{i}} dy_{i} \right). \tag{60}$$

The differentials of phase amount and site fraction are included because at equilibrium they are dependent variables which are functions of T. Thus, in order to claim that

$$\frac{dG}{dT} = \sum \mathcal{N}^{\alpha} \frac{\partial G_M^{\alpha}}{\partial T},\tag{61}$$

it needs to be shown that

$$\sum_{i} \mathcal{N}^{\alpha} \sum_{i} \frac{\partial G_{M}^{\alpha}}{\partial y_{i}} dy_{i} + \sum_{i} G_{M}^{\alpha} d\mathcal{N}^{\alpha} = 0.$$
 (62)

Substituting the differential form of M^α_A as a function of dy_i given in Eq. (29) into the differential form of G^α_M given in Eq. (36) results in

$$dG_{M}^{\alpha} = \frac{\partial G_{M}^{\alpha}}{\partial T} dT + \frac{\partial G_{M}^{\alpha}}{\partial P} dP + \sum_{i} \sum_{A} \mu_{A} \frac{\partial M_{A}^{\alpha}}{\partial y_{i}} dy_{i}.$$
 (63)

Inspection of Eq. (63) reveals

$$\frac{\partial G_M^{\alpha}}{\partial y_i} = \sum_A \mu_A \frac{\partial M_A^{\alpha}}{\partial y_i},\tag{64}$$

and the combination of Eqs. (29) and (64) shows

$$\sum_{i} \frac{\partial G_{M}^{\alpha}}{\partial y_{i}} dy_{i} = \sum_{i} \sum_{A} \mu_{A} \frac{\partial M_{A}^{\alpha}}{\partial y_{i}} dy_{i} = \sum_{A} \mu_{A} \sum_{i} \frac{\partial M_{A}^{\alpha}}{\partial y_{i}} dy_{i} = \sum_{A} \mu_{A} dM_{A}^{\alpha}.$$
(65)

Application of Eq. (65) to the left-hand side of Eq. (62) gives the expression

$$\sum_{\alpha} \mathcal{N}^{\alpha} \sum_{A} \mu_{A} dM_{A}^{\alpha} + \sum_{\alpha} G_{M}^{\alpha} d\mathcal{N}^{\alpha}. \tag{66}$$

Now, because the system is assumed to be closed, the differentials of the moles of components are set equal to zero, and manipulation of Eq. (27) reveals that for any component A

$$\sum_{\alpha} d\mathcal{N}^{\alpha} M_{A}^{\alpha} = -\sum_{\alpha} \mathcal{N}^{\alpha} dM_{A}^{\alpha}. \tag{67}$$

Substituting this information into the first term of the expression in Eq. (66) and applying Eq. (2) gives

$$-\sum_{\alpha}d\mathcal{N}^{\alpha}\sum_{A}\mu_{A}M_{A}^{\alpha}+\sum_{\alpha}G_{M}^{\alpha}d\mathcal{N}^{\alpha}=-\sum_{\alpha}G_{M}^{\alpha}d\mathcal{N}^{\alpha}+\sum_{\alpha}G_{M}^{\alpha}d\mathcal{N}^{\alpha}=0, \eqno(68)$$

proving that Eq. (62) is indeed true.

Appendix B. Supplementary data

Supplementary material related to this article can be found online at https://doi.org/10.1016/j.calphad.2024.102705.

References

- [1] N. Saunders, A.P. Miodownik, CALPHAD (Calculation of Phase Diagrams): A Comprehensive Guide, Elsevier, 1998.
- [2] J.-O. Andersson, T. Helander, L. Höglund, P. Shi, B. Sundman, Thermo-Calc & DICTRA, computational tools for materials science, CALPHAD 26 (2) (2002) 273–312.
- [3] B. Jansson, Physical Metallurgy (Ph.D. thesis), KTH Stockholm, Sweden, 1984.
- [4] B. Sundman, U.R. Kattner, M. Palumbo, S.G. Fries, OpenCalphad-A free thermodynamic software, Integr. Mater. Manuf. Innov. 4 (2015) 1–15.
- [5] R. Otis, Z.-K. Liu, Pycalphad: CALPHAD-based computational thermodynamics in Python, J. Open Res. Software 5 (1) (2017).
- [6] H. Larsson, M. Jansson, Rate of change at equilibrium, CALPHAD 51 (2015)
- [7] B. Sundman, X.-G. Lu, H. Ohtani, The implementation of an algorithm to calculate thermodynamic equilibria for multi-component systems with non-ideal phases in a free software, Comput. Mater. Sci. 101 (2015) 127–137.
- [8] Y. Cao, S. Li, L. Petzold, R. Serban, Adjoint sensitivity analysis for differentialalgebraic equations: The adjoint DAE system and its numerical solution, SIAM J. Sci. Comput. 24 (3) (2003) 1076–1089.
- [9] H. Lukas, J. Weiss, E.-T. Henig, Straegies for the calculation of phase diagrams, CALPHAD 6 (3) (1982) 229–251.
- [10] M. Hillert, Some viewpoints on the use of a computer for calculating phase diagrams, Physica B+ C 103 (1) (1981) 31–40.
- [11] W. Alt, K. Malanowski, The Lagrange-Newton method for nonlinear optimal control problems, Comput. Optim. Appl. 2 (1993) 77–100.
- [12] R. Otis, B. Bocklund, Z.-K. Liu, Sensitivity estimation for calculated phase equilibria, J. Mater. Res. 36 (2021) 140–150.
- [13] N. Ury, R. Otis, V. Ravi, Generalized method of sensitivity analysis for uncertainty quantification in Calphad calculations, CALPHAD 79 (2022) 102504.
- [14] J.P.S. Palma, R. Gong, B.J. Bocklund, R. Otis, M. Poschmann, M. Piro, S. Shahbazi, T.G. Levitskaia, S. Hu, N.D. Smith, et al., Thermodynamic modeling with uncertainty quantification using the modified quasichemical model in quadruplet approximation: Implementation into PyCalphad and ESPEI, CALPHAD 83 (2023) 102618.
- [15] B. Bocklund, R. Otis, A. Egorov, A. Obaied, I. Roslyakova, Z.-K. Liu, ESPEI for efficient thermodynamic database development, modification, and uncertainty quantification: Application to Cu–Mg, MRS Commun. 9 (2) (2019) 618–627.
- [16] E. Galvan, R.J. Malak, S. Gibbons, R. Arroyave, A constraint satisfaction algorithm for the generalized inverse phase stability problem, J. Mech. Des. 139 (1) (2017) 011401.

- [17] A. Abu-Odeh, E. Galvan, T. Kirk, H. Mao, Q. Chen, P. Mason, R. Malak, R. Arróyave, Efficient exploration of the high entropy alloy composition-phase space, Acta Mater. 152 (2018) 41–57.
- [18] M. Hillert, The compound energy formalism, J. Alloys Compd. 320 (2) (2001) 161–176.
- [19] PyCalphad pull request #517. URL https://github.com/pycalphad/pull/517.
- [20] PyCalphad pull request #432. URL https://github.com/pycalphad/pull/432.
- [21] C.R. Harris, K.J. Millman, S.J. van der Walt, R. Gommers, P. Virtanen, D. Cournapeau, E. Wieser, J. Taylor, S. Berg, N.J. Smith, R. Kern, M. Picus, S. Hoyer, M.H. van Kerkwijk, M. Brett, A. Haldane, J.F. del Río, M. Wiebe, P. Peterson, P. Gérard-Marchant, K. Sheppard, T. Reddy, W. Weckesser, H. Abbasi, C. Gohlke, T.E. Oliphant, Array programming with NumPy, Nature 585 (7825) (2020) 357–362, http://dx.doi.org/10.1038/s41586-020-2649-2.
- [22] M. Seiersten, in: I. Ansara, A. Dinsdale, M. Rand (Eds.), COST 507, Thermochemical Database for Light Metal Alloys, vol. 2, Office for Official Publications of the European Communities, 1998.
- [23] S. Sheikh, M. Ranaiefar, P. Honarmandi, B. Vela, P. Morcos, D. Shoukr, R. Arroyave, I. Karaman, A. Elwany, An automated fully-computational framework to construct printability maps for additively manufactured metal alloys, 2023, arXiv preprint arXiv:2304.04113.
- [24] S. Sheikh, B. Vela, P. Honarmandi, P. Morcos, D. Shoukr, A.M. Kotb, R. Arroyave, I. Karaman, A. Elwany, High-throughput alloy and process design for metal additive manufacturing, 2023, arXiv preprint arXiv:2304.04149.
- [25] K. Karayagiz, A. Elwany, G. Tapia, B. Franco, L. Johnson, J. Ma, I. Karaman, R. Arróyave, Numerical and experimental analysis of heat distribution in the laser powder bed fusion of Ti-6Al-4V, IISE Trans. 51 (2) (2019) 136–152.
- [26] X. Huang, J. Berry, A. Perron, R. Arróyave, A comparative study of Kim-Kim-Suzuki (KKS), partition coefficient relaxation (PCR), and finite interface dissipation (FID) phase field models for rapid solidification, Addit. Manuf. 74 (2023) 103704.
- [27] A. van de Walle, S. Samanta, C. Nataraj, S. Zhu, H. Chen, H. Liu, R. Arroyave, Revisiting the SGTE lattice stability of bcc aluminum, CALPHAD 83 (2023) 102628.
- [28] A. Van De Walle, R. Sun, Q.-J. Hong, S. Kadkhodaei, Software tools for high-throughput CALPHAD from first-principles data, CALPHAD 58 (2017) 70–81
- [29] M. Poschmann, M.H. Piro, T.M. Besmann, K.T. Clarno, S. Simunovic, Thermochemically-informed mass transport model for interdiffusion of U and Zr in irradiated U-Pu-Zr fuel with fission products, J. Nucl. Mater. 554 (2021) 153089.
- [30] M. Piro, S. Simunovic, T.M. Besmann, B. Lewis, W. Thompson, The thermochemistry library thermochimica, Comput. Mater. Sci. 67 (2013) 266–272.
- [31] J. Hales, R. Williamson, S. Novascone, G. Pastore, B. Spencer, D. Stafford, K. Gamble, D. Perez, W. Liu, BISON Theory Manual the Equations Behind Nuclear Fuel Analysis, Tech. Rep., Idaho National Lab.(INL), Idaho Falls, ID (United States), 2016.
- [32] E. Povoden-Karadeniz, D. Cirstea, P. Lang, T. Wojcik, E. Kozeschnik, Thermodynamics of Ti–Ni shape memory alloys, CALPHAD 41 (2013) 128–139.
- [33] Z. Rao, B. Dutta, F. Körmann, W. Lu, X. Zhou, C. Liu, A.K. da Silva, U. Wiedwald, M. Spasova, M. Farle, et al., Beyond solid solution high-entropy alloys: Tailoring magnetic properties via spinodal decomposition, Adv. Funct. Mater. 31 (7) (2021) 2007668.
- [34] Y. Chen, Y. Fang, R. Wang, Y. Tang, S. Bai, Q. Yu, Achieving high strength and ductility in high-entropy alloys via spinodal decomposition-induced compositional heterogeneity, J. Mater. Sci. Technol. 141 (2023) 149–154.